Graduate Theses and Dissertations   Graduate School

2008

Microsphere-aided characterization of stimuli-responsive polymer networks

Carlos A. Bello
University of South Florida

Follow this and additional works at: http://scholarcommons.usf.edu/etd

Part of the American Studies Commons

Microsphere-Aided Characterization of Stimuli-Responsive Polymer Networks

by

Carlos A. Bello

A thesis submitted in partial fulfillment
of the requirements for the degree of
Master of Science in Chemical Engineering
Department of Chemical & Biomedical Engineering
College of Engineering
University of South Florida

Major Professor: Ryan G. Toomey, Ph.D.
John T. Wolan, Ph.D.
Martin Muschol, Ph.D.

Date of Approval:
November 5, 2008

Keywords: soft lithography, confocal microscopy, microstructures, poly(NIPAAm), Delaunay triangulation

DEDICATION

To my mom

ACKNOWLEDGEMENTS

First, I wish to sincerely thank my Professor, Dr. Toomey for guiding me throughout my research and providing valuable insight over the past three years. It is because of Dr. Toomey's advice and support that my graduate career has been rewarding. I will always be grateful for the time he took to enhance my knowledge and understanding on a wide variety of topics, which have all been vital to the success of my graduate studies. I am also grateful to Samuel DuPont for his continued support, as well as Dr. Wang's group, who manufactured the SU-8 molds. Thanks to my committee members, Dr. Wolan and Dr. Muschol, who have played an integral part in my graduate education. A special thanks to my lab partners who have played an integral part in my graduate education: Mr. Ajay Vidyasagar, Ms. Leena Patra, Ms. Ophir Ortiz, Ms. Chamila Siyambalapitiya, Mr. Ryan Cates, Ms. Gulnur Efe and Mr. Abiola Shitta.

TABLE OF CONTENTS

ii

LIST OF TABLES

LIST OF FIGURES

iv

v

Microsphere-Aided Characterization of Stimuli-Responsive Polymer Networks

Carlos A. Bello

ABSTRACT

The fabrication and characterization of surface-anchored hydrogel microstructures are described. The hydrogel structures are constructed from poly(N-isopropylacrylamide), or poly(NIPAAm), which is a well-known thermoresponsive polymer that swells and contracts with changes in temperature. When patterned on a surface, these structures can experience a variety of shape changes induced by nonuniform swelling. Depending on the aspect ratio, patterns can, for instance buckle upon swelling and form wave-like patterns. Such structural changes replicate oscillatory motion of the smooth muscle cells and can be used to transport objects in microfluidics. The work, herein, investigates methods of pattern production and introduces a new technique for characterizing local swelling in the patterns. In order to achieve the latter, fluorescent microspheres were embedded in hydrogel patterns and their positions were mapped in three-dimensions using confocal microscopy. The

measurements permit, for the first time, swelling maps of the structures based on relative movements of the microspheres. This information will ultimately aid in understanding how swollen macroscopic structures are related to gradients in localized swelling.

CHAPTER ONE: INTRODUCTION

The set of techniques used for the fabrication of patterned poly(N-isopropylacrylamide), poly(NIPAAm), hydrogel microstructures on glass substrate, and the methods for measuring the local swelling inside a hydrogel structure are describe here. Poly(NIPAAm), is a well-know thremoresponsive polymer that exhibits a lower critical solution temperature (LCST) when mixed with water,[1] wherein the polymer phase separates above the LCST. The transition temperature can also be affected by the addition of salt, alcohol, pH and surfactants.[2] The unusual phase behavior is a consequence of the entropy gain accompanying dehydration of the amide moieties above the LCST. For cross-linked gels, the LCST results in shrinkage in size. These materials have been of great interest in applications such as chemical/biological sensors, drug delivery, biomaterials, and chemical/biological separations.[3, 4]

There is a growing interest in using patterned poly(NIPAAm) microgels in microfluidics for their actuation properties. However, there are no techniques to characterize local swelling of surface-attached networks while the swelling of unconfined networks is well understood (see Figure 1-1). Surface-attachment of network results in non-uniform swelling that leads to a variety of swollen structures (see Figure 1-1 and Figure 1-2).

The polymer trenches were fabricated by a technique employing soft lithography. Soft lithographic methods use an elastomeric stamp or mold prepared by casting the liquid prepolymer of an elastomer against a master that has a patterned relief structure.[5] Glass surfaces were first acrylated with a trichlorosilane surface attach monolayer (SAM) to ensure covalent attachment of the poly(NIPAAm) arrays and thereby improve hydrogel adhesion to the substrate. A poly(NIPAAm) hydrogel containing 0.005 wt% of fluorescent microspheres was polymerized onto the treated substrate. As a result, three-dimensional, cross-linked poly(NIPAAm) hydrogel microstructures were attached to the surface. Widths and gaps between the structures were varied from 5 – 20 µm by the use of different patterns in a photo mask, while height varied from 5 – 25 µm, depending on the SU-8 photoresist used (SU-8 2025 or SU-8 2005). The hydrogel patterns were hydrated for as long as 2 weeks without any notice of delamination from the substrate.

When the hydrogel structures are below the LCST, they form either a wave-like pattern known as buckling or a mushroom-like shape.[6] The contraction/swelling behavior of the trenches was characterized with spinning-disk confocal microscopy, SDCM.

This thesis presents an approach to soft lithography making micrometer-scale patterns of poly(NIPPAm) hydrogel monoliths with embedded fluorescent microspheres on solid surfaces in order to characterize the swelling behavior of the gel.   Whereas mechanically pinning a polymer hydrogel to a surface

generally confines swelling in the usual direction, adequately high aspect ratios allow lateral swelling to the surface. This type of swelling makes possible the creation of "intelligent" surfaces, described previously by Castellanos (2007). In addition, a set of imaging processing steps is described here in order to directly quantify the local spatial structure of the surface-attached hydrogels by measuring the distribution of the microspheres inside the polymer.
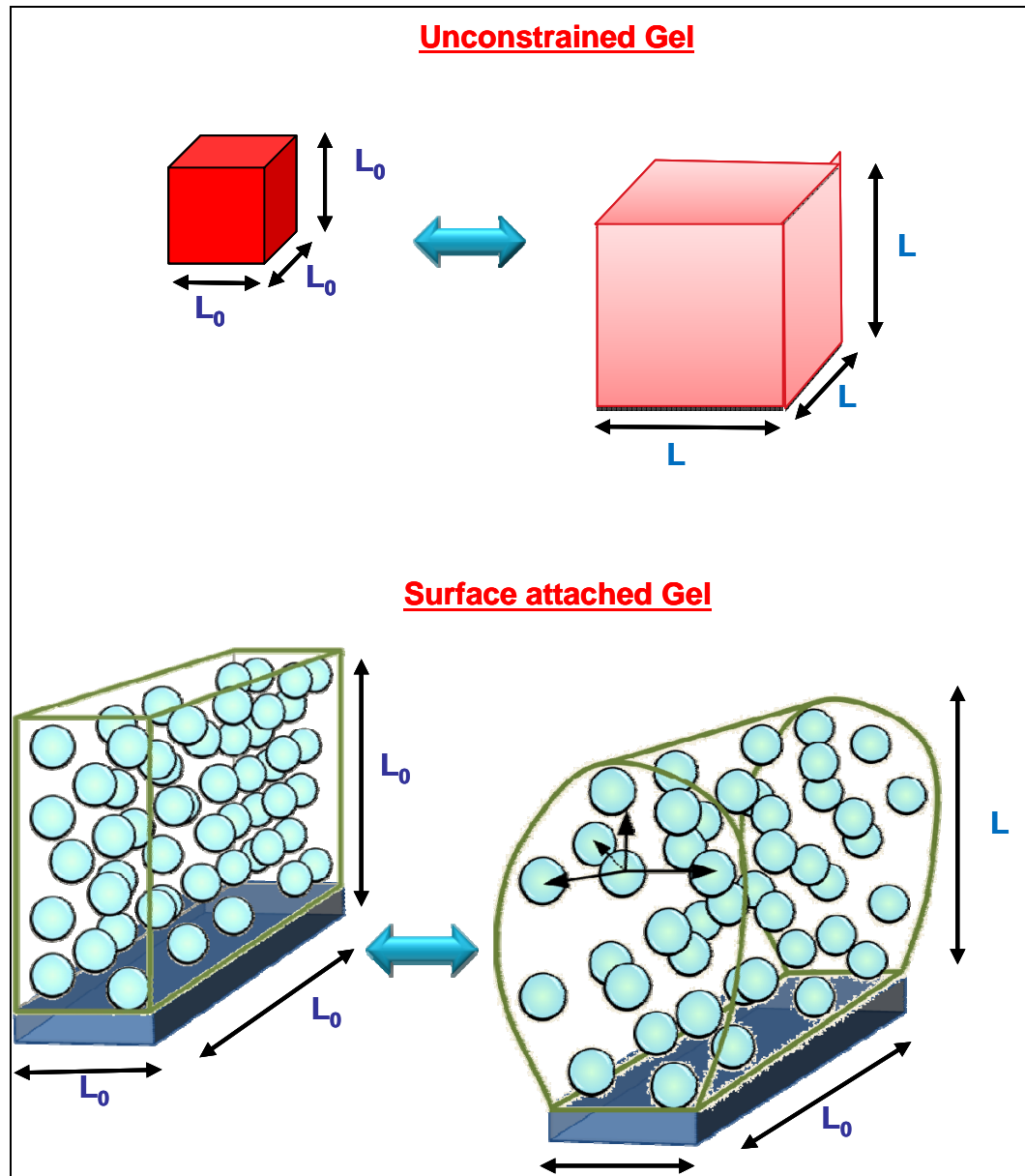
Figure 1-1. Swelling behavior: unconstrained gels vs. surface attached gels

Mold: Heigh um	Mold: gap um	Mold: width um		Mold: Heigh um	Mold: gap um	Mold: width um
25	15	10	Below LCST	5	15	10

20 μm

15 μm

Above LCST

20 μm

15 μm
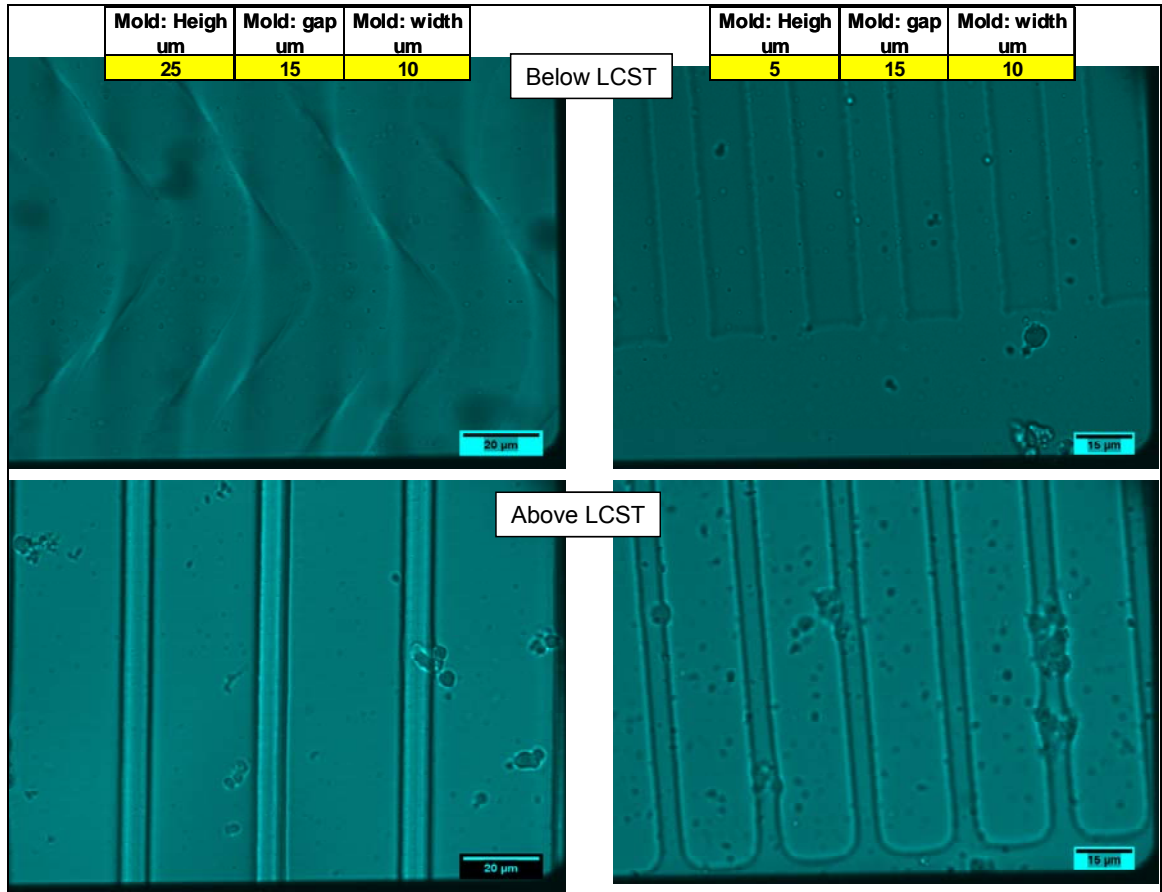
Figure 1-2. Microstructures of poly(NIPAAm) below and above LCST

CHAPTER TWO: FABRICATION OF POLY(NIPAAM) MICROSTRUCTURES

Thick (>100 μm), high aspect-ratio microstructures have traditionally been developed by using LIGA microstereo lithography [7] and deep reactive ion etching (DRIE) processes.[8, 9] However, the problem with these techniques is that they often involve equipment that is not readily available due to its complexity, and as a result, is expensive. On the other hand, the techniques used for soft lithography are relatively inexpensive, and the procedures used are relatively easy since it can be done in the laboratory. Soft lithography creates by contact printing micropatterns of self-assembled monolayers, SAMs,[10] which occurs when molecules or objects spontaneously organize into steady, well-defined structures by non covalent forces.[11] Finally, soft lithography does not have all of the limitations that optical diffraction and optical transparency have.[12]

The technique used to make microfluidic channels during this research was based on the patterning of SU-8 photoresist. The properties of these SU-8 photoresist patterning have made possible to create many new microfluidic devices, whose capabilities have been well demonstrated.[13] On the other hand, PDMS was used as the elastomer for the majority of the research associated with soft lithography. PDMS has several properties that make it well suited for soft-lithography, such as its biocompatibility, permeability to gases, as well as its

www.manaraa.com

ability to be use with cell cultures.[14] In addition, PDMS is see-through above 300 nm, and since it is elastomeric, it can reach non planar surfaces conformably.[15]

Once the photoresist patterns are layered on silicon substrates using soft lithography, they can be uses as masters to make the necessary PDMS stamps. Glass surface was treated with 3-(trichlorosilyl)propyl methacrylate to create a SAM with pendant acrylate groups. Glass surfaces or silicon were first acrylated with a trichlorosilane SAM to ensure a covalent connection of the PEG arrays and thus strengthen hydrogel adhesion to the substrate.[16] Micropatterned substrates were set up by the photopolymerization of NIPAAm onto surfaces functionalized with 3-(trichlorosilyl)-propyl methacrylate monolayer. These surfaces ensured the attachment of the hydrogel to the substrate as well as allowing for cell adhesion in areas lacking hydrogel as a result of its hydrophobicity.[17]

The production of high-aspect ratio microfluidic channels is still under extensive research. SU-8 is an epoxy-based line of near-ultraviolet (UV) radiation-sensitive photoresists. It has high contrast, as well as suitable chemical and mechanical properties, which are capable of developing thick photoresist structures in a single photolithographic step.[18] SU-8 photoresists have yielded aspect ratios of over 25 [19, 20] and microstructures up to 1.5 mm high using a single coating step.[21]

7

Soft lithography techniques have yielded results which include very high aspect-ratio micro-structures with vertical sidewalls and high resolution.[22] Various groups have found that a micro-structure 1.2 mm in height can be formed by double coating the SU-8 photoresist layers [13]. Multicoating, on the other hand, is a very time-consuming process. The use of NANOTM SU-8 (MicroChem Corp., Newton, MA) photoresist to increase thick microstructures for MEMS has drawn significant attention.[18, 21, 23] Another process that is used to generate complex SU-8 features is the creation of multi-level microstructures by performing various photolithographic steps of exposure and development.[24] For example, the spinning and exposing of multiple layers of SU-8 sequentially followed by a simultaneous (single) developing step have achieved both, two and three-level microstructures.[25, 26]

One drawback associated with the use of SU-8 photoresist is related to stress, adhesion selectivity, and resist stripping. During the development process, the SU-8 photoresist can simply be removed from the surfaces of such materials. The thermal expansion coefficient mismatch is large on many surfaces, such as silicon or glass, which are suitable for spinning the SU-8 photoresist. This results in a large amount of stress at the material interface, due to the size reduction of the SU-8 photoresist while cross-linking during curing. The stress effect is pronounced in large SU-8 photoresist structures and, if poor adhesion is obtained during processing, the photoresist delaminates easily. Coating, baking, the developing efficiency, and the tremendous residual stress

8

formed after curing are just some of the challenges involved in making an ultra-thick micro-structure with SU-8 photoresist. The flatness of the surface is also a major issue. SU-8 photoresists present many challenges despite its popularity. For instance, it hinders reproduction and limits potential applications.[21, 27, 28] Furthermore, differences in exposure throughout the photoresist layer can result in partial curing of the resist, residual stress build-up, as well as poor adhesion to the underlying silicon wafer. This can result in distortions, such as lifting off the entire SU-8 pattern.[21, 25-27, 29-31] The consistency of exposure provided by an appropriate contact between the photoresist and mask is particularly important for thicker SU-8 layers and is highly reliant on other processing steps.[21] First, the variations of thickness in the SU-8 layer across the wafer is a result of flowing of the uncross linked photoresist during the soft-bake step.[21, 29] Secondly, the creation of edge beads during the spin coating procedure likewise produces variations in thickness across the wafer. Third, multiple SU-8 layers can enhance residual stresses, as well as subsequent bowing of the silicon wafer.[18, 21, 29, 32] Components of the developing step also play a crucial role in the processing of SU-8 microstructures (see Figure 2-1). Whereas low-aspect ratio features are typically insensitive to developing parameters, high-aspect ratio microstructures many times require optimization of the development time as well as the use of agitation.[32] On the other hand, forceful agitation of the SU-8 Developer could lead to the destruction of high aspect ratio structures.[33]

9

2.1. Photolithography Process

Two types of photoresists were used to fabricate different thicknesses of SU-8 structures. SU-8 2005 produces 3 – 7.5 μm structures, and SU-8 2025 produces 20 – 75 μm structures.

2.1.1. Piranha Clean

In order to start the photolithography process, it is best to clean and dry substrates before using SU-8 resist. Doing so will provide maximum process reliability. For the most accurate results, substrates should be cleaned with a piranha wet etch, using H_2O_2 and H_2SO_4, along with a de-ionized water rinse. The n-type <100> Single-Side-Polished 2" silicon wafers were cleaned with a piranha solution, which removes organic material from substrates. Piranha cleaning solution is a warm mixture of sulfuric acid (H_2SO_4) and hydrogen peroxide (H_2O_2) typically at 100 ^oC – 150 ^oC, this mixture reacts violently with organic materials and must be handled with extreme care. Therefore, it is performed in a glass container with extra protective equipment like rubber gloves, heavy apron with sleeves, and full-face shield in addition to safety glasses. Moreover, this process is performed in a well-ventilated wet bench. The H_2SO_4 to H_2O_2 ratio is 3:1, and once the H_2SO_4 is added to H_2O_2 the reaction must be allowed to occur within a time range of 1 to 2 minutes. Next, the silicone wafers are slowly added to the solution and allowed to develop for 10 minutes. Once

10

the silicone wafers have fully developed, they must be removed. Excess rinsing with de-ionized water is required in order to remove excess amount of acidic residue; consequently, achieving a surface that is free of excess acidic remains. Once all excess acidic remains have been removed, the silicone wafers must be allowed to dry with a continuous flow of nitrogen.

2.1.2. Dehydration Bake

For the soft bake process, a level hotplate should be used. It is important to use one with good thermal control, as well as uniformity. The vendor does not recommend the use of convectional ovens. The dehydration bake was performed for 10 mins at 150 ^{o}C.

The wafer should be removed from the hotplate after the allotted time. This will help optimize the baking conditions. Once it has cooled to room temperature, it should be returned to the hotplate. In the event that the film 'wrinkles', the wafer should be put back on the hotplate for a couple of more minutes. The same cool down and heat up cycle should be repeated until the wrinkles are no longer visible in the film.

11

2.1.3. Coat

The purpose of spin coating is to apply a uniform layer of SU-8 over the entire surface of the silicone wafer. A 2 ml pipette was used in the first attempt to make a smooth layer of the SU-8. A small amount of acetone was applied to the edge of the wafer to eliminate the excess build-up of photoresist accumulated throughout the various spinning cycles. The elimination of excess edge bead allows the mask to be put in close contact with the silicone wafer, thus enhancing the resolution.

SU-8 2000 is best when used for imaging near vertical sidewalls in thick films. This is due to its high optical transmission, which is above 360 nm. Some of the many features of the SU-8 2000 include high aspect ratio imaging, vertical sidewalls, improved coating properties, and 0.5 to > 200 µm film thickness in one coat. A spin coater Model p6700 is used for the coating of the photoresist.

The MicroChem recommended coating conditions are as follows:

- STATIC Dispense: Approximately 1ml of SU-8 2000 per inch of substrate diameter.
- Spread Cycle: Increase to 500 rpm at 100 rpm/second acceleration. This will take 5 seconds.
- Spin Cycle: Increase to final spin speed at an acceleration of 300 rpm/second and maintain at said rate for a total of 30 seconds.

12

There were some challenges in the coating of the SU-8 which affected the consistency of the results from experiment to experiment. It was found that pulling photoresist directly from bottle reduced the formation of bubbles on top of the surface. In addition, a high acceleration (>10,000 rpm/sec) seemed to be more favorable for a better spreading of the SU-8. Also, there were some samples done with an expired SU-8 which generated ticker structures. Finally, the photoresist should be kept inside the fridge. However, it was observed that when it was spin at cold temperatures it gave unpredicted results. Therefore, the SU-8 needs to be at room temperature when it is spin coat.

2.1.4. Soft Bake

A level hotplate should be used during this process. It is also important to use one that has good thermal control, as well as uniformity. Since it is possible for a skin to form on the resist, the vendor strongly advises against using convection ovens. The formation of this skin could in turn stop the evolution of solvent, which would either prevent the film from drying or lead to an extended bake time. Table 2-1 lists what is recommended for the soft bake times and temperatures for the used SU-8 2000 products based on the selected film thicknesses.

13

Table 2-1. Recommended soft bake parameters

Product Name	Thickness (um)	Pre-bake @ 65 ^{o}C	Soft bake @ 95 ^{o}C
SU-8 2005	3	1	2
	5	1	2
	6	1	2
	7.5	1	2
SU-8 2025	20	2	5
	75	3	9

In order to prevent any complications with step coverage on the silicon, the sample was given an hour to relax once the spin coating was complete. A pre-exposure bake was done by extending and increasing the temperature as a means to reduce stress and to permit solvent evaporation. The sample was baked on a hotplate at 65 ∘C for 5 minutes. The temperature was immediately increased, and baking continued at 95 ∘C for 40 minutes.

Soft bake process:

- 65 ∘C for 1 min on the hot plate,

- 95 ∘C for 5 min in the oven,

- 10 min of cool down period (relaxation) at room temperature (~25 ∘C).

It is worth mentioning some of the challenges and conclusions of the soft bake step. It is better to use soft bake times for high aspect ratio to reduce the retained solvent level since doing so can lessen the risk of exposed resist loss, adhesion failure, and swelling. It is possible that a build-up of photoresist could form around the edge of the substrate during the spin coat process.

14

2.1.5. Exposure

The mask was design on AutoCAD by another group member. The color of the mask body is black for the most part and will not absorb the UV light. Even still, only the see-through areas of the mask will absorb the UV light and, as a result, become a permanent fixture.

A Karl Suss Mask Aligner UV light source was used for exposure. A mask, which defined the locations of the SU-8 photoresist on the wafer, was used, while exposure continued for 35 seconds. The SU-8 photoresist structures on the cantilevers formed the trenches.

In order to eliminate the UV radiation below 350 nm a Hoya UV-34 filter has been used. Excessive dose below 350nm may has been proven to result in over exposure of the top portion of the resist film, resulting in exaggerated negative sidewall profiles or T-topping.[34] In addition, Chuang (2005) showed that smaller and uniform gap between photomask and resist reduced the diffraction error.[28] He proved that the edges of mask patterns usually pose diffraction effect during contact printing, which is produced by Fresnel diffraction. When the thickness of photoresist and the gap between photomask and resist increases, the diffraction error gets larger. Consequently, it results in non-straight sidewall of resist structures and constrains the application of microstructures in high-aspect-ratio range.[28] Revzin (2001) used contact printing to reduced the diffraction caused by the air gap.[16] According to Revzin (2001), the square root of the gap

15

between a photomask and polymer layer is directly proportional to the minimum resolution.[16] Consequently, the gap has to be minimized in order to get images at resolutions critical to our experiments.

The exposure time (dose) has been varied to obtained different thicknesses. Besides, it is well known from literature that ticker films require higher dosage. The exposure process was initiated by having a vacuum contact between the mask and the silicon wafer. Then the UV filter was located between the UV source and the mask. Finally, 100 mJ (10.0 mW cm^{-2} for 10.0 s or 15.0 mW cm^{-2}) were applied to the substrate.

The thickness non-uniformity caused by standard resist spinner and hot plate soft-baker can easily pose 30–100 μm air gap when contacting with photomasks for resist thickness ranging from 0.1 to 1 mm. Printing mask pattern through the aforementioned air gap causes the resulting patterns deform. The key phenomenon that affects the size of patterns and sidewall profile in the UV lithography printing is the Fresnel diffraction which gives more energy on the pattern edges.[28]

Chuan (2002) described a novel way to compensate the air gap between photomask using glycerol between the mask and the sample. This technique highly reduced the UV light diffraction on photoresist. Also, this method increases the side wall straightness.[28]

16

2.1.6. Post Exposure Bake (PEB)

Post exposure bake (PEB) was carried out at 65 ^{o}C for 3 minutes and 95 ^{o}C for 12 minutes. After this, the samples were left at room temperature to avoid excess stress due to thermal gradients.

It was concluded that extended PEB times at lower temperatures give better results than the samples treated at higher temperatures. In addition, an image of the mask should be seen in the photoresist coating after one minute of PEB, which indicated that there was insufficient exposure, heating or both.

2.1.7. Development

The development process consists of gentle agitation for 8 minutes. The substrates were developed using a MicroChem SU-8 photoresist developer. This step clears out deep trenches. Various techniques were tested before finding a suitable technique for the patterning requirements. For example, one technique in particular consisted of placing the wafer on a stir rod and then immersing it in developer. The problem with this, however, is that a significant amount of heat is absorbed when drying the acetone that the temperature of the substrate drops significantly. This, in turn, could either cause extreme thermal expansion or contraction. In either case, this will cause stress cracks to the film. Finally, the samples were heated on the hotplate at 15 ^{o}C for 1 min after development.

17

If, during the IPA rinse, a white film is formed, it means that the unexposed photoresist was underdeveloped. A quick fix would be to add more SU-8 developer to the substrate. Doing so will remove the white film and finish the development process. Rinse steps should be repeated.

In order to dry the sample it is important to keep the patterned face of the wafer away from strong nitrogen flow currents since these blows of nitrogen can delaminate the SU-8 in this step of the process. Therefore, it is important to blow dry the back side of the wafer in order to dry it, and then it is necessary to put the wafer in a spin coater and spin it dry at 2000-3000 rpm for about 15 seconds. Figure 2-2 shows each step of the entire photolithography process.

2.2. Silicon-PDMS Molding

Soft lithographic methods use an elastomeric stamp or mold, prepared by casting the liquid prepolymer of an elastomer against a master that has a patterned relief structure.[5] Most of the research based on soft lithography has used poly(dimethylsiloxane) (PDMS) as the preferred elastomer. PDMS has become the primary material for the low-volume manufacturing of microfluidic devices owing to its ease of processing in standard laboratory conditions, and low cost. In addition, PDMS has several properties that make it well suited for patterning proteins and cells. It is biocompatible, permeable to gases, and can be

18

used for cell culture. Furthermore, it is optically transparent down to about 300 nm, and it can contact non-planar surfaces conformably due to its elasticity.[5]

The elastic characteristic of PDMS allows it to be released easily, even from complex and fragile structures. Also, PDMS provides a surface that is low in interfacial free energy (ca. 21.6×10^{-3} Jm^{-2}) and chemically inert.[12]

Finally, it has been shown that three-dimensional structures can be built up layer by layer, e.g. fluidic channels and mixers,[35, 36] valves,[37] and pumps connected to an active microfluidic matrix to perform programmable tasks[38] with the use of the PDMS elastomer. The fabrication of the SU-8 patterned photoresist structures was discussed in previous sections. These masters were used for PDMS embossing.

A mix of PDMS, (Dow Corning), and curing agent was prepared in a 10:1 ratio. The prepolymer mixture was degassed with a mechanical vacuum pump to remove any air bubbles in the mixture and to insure complete mixing between the two parts[5] (see Figure 2-3, which shows a PDMS molds that was not degassed with the mechanical pump). The PDMS mix was placed on top of the patterned SU-8 photoresist and placed on a hot plate at 75 ^{O}C for 60 minutes in order to obtain the solidified PDMS mold. Afterwards, the sample was allowed to cool down for 2 hours in order to obtain the desired final patterns. Finally, excess PDMS was cut off at the edges in order to expose the openings of the channels;

19

this is done in order to apply capillary force to the pre-polymer solution (see Figure 2-4 and Figure 2-5 for a detail illustration of the process).

The elastomeric character of PDMS is also the origin of some of the most serious technical problems that must be solved before soft lithography can be used in forming complex patterned structures. For instance, PDMS molds were not release easily from the silicon wafers even though of its elasticity and low surface energy. After curing the PMDS, this was peeled out from the mold revealing the microfluidic channels. Observations in a conventional microscope before and after the peeling of the PDMS (not shown in this thesis) points up the destruction of the PDMS mold. Therefore, special attention was taken during this process in order to minimize this destruction.

There are several other disadvantages that may limit the performance of PDMS for certain types of applications. For example, PDMS shrinks by a factor of about 1% upon curing.[12] Also, gravity, adhesion and capillary forces exert stress on the elastomeric features and cause them to collapse and generate defects in the pattern that is formed.[39] This could occur, for example, if the aspect ratio of the relief features is too large. Then the PDMS microstructures could collapse or fall under their own weight; Delamarche (1997) showed that the aspect ratios of the relief structures on PDMS surfaces had to be between about 0.2 and 2 in order to obtain defect-free stamps.[39] On the other hand, when the aspect ratio is too low, insufficient relief exists on the surface of the stamp to

20

withstand the compressive forces (due to adhesion between stamp and substrate) typical of printing.

2.3. Silanization of Glass Substrates

In early experiments poly(NIPAAm) microstructures were generated on glass surfaces cleaned with Acetone/Methanol/IPA but not modified with and adhesion promoting monolayer. Even though patterns could be develop, surface attachment was weak and microstructures easily delaminated upon hydration due to swelling of the cross-linked polymer. A slightly better attachment of the network was obtained by treating the substrate with 3-aminopropyl triethoxysilane. However, by using a self assembled monolayer of 3-(trichlorosilyl)propyl methacrylate (TPM, Aldrich) a reactive surface was covalently affixed to the gel during photopolymerization, which prevented delamination.

The treatment of glass surfaces with chlorosilanes or alkoxysilanes is a very common and effective way to form dense, self-assembled monolayers.[40, 41] In order to ensure covalent attachment of the poly(NIPAAm) arrays and thereby improve hydrogel adhesion, an adhesion layer was created using a monolayer of TPM. The modification of the substrates was performed using standard protocols for silane surface modifications.[42] In brief, cover slides were cleaned with the standard solvent cleaning process using Acetone/Methanol/IPA and DI water.

21

Subsequently, in order to remove organic contaminants and to promote hydroxylation (OH groups) on the surface, the cover slides were plasma-cleaned (Harrick Plasma Cleaner/Sterilizer PDC-32G) for 10 minutes at 1 Torr with a medium RF power. During this process organic contaminants are removed by chemical reaction with highly reactive oxygen radicals and ablation by energetic oxygen ions. Substrates were then treated for 5 min, at room temperature, in a 1 mM solution of TPM in a 4:1 ratio of heptane-carbon tetrachloride in an N_2 atmosphere, followed by washing with hexane and water. Figure 2-6 depicts the silanization mechanism of glass surfaces.

2.4. Photopolymerization of Hydrogel with Embedded Microspheres

N-isopropylacrylamide (NIPAAm) (97% Aldrich) was recrystallized from n-hexane solution. The crosslinking agent was *N*, *N* – methylenebisacrylamide (BIS, Chemzymes Ultra Pure). The initiator for the polymerization reaction was 2-dimethoxy-2-phenylacetophenone (DMPA, Aldrich). 500 nm polystyrene yellow-green fluorescence microspheres (Molecular Probes, Invitrogen, CA) were used as molecular probes.

Once the surface of the coverslip is treated with the silane binder, PDMS is placed on the surface of the substrate. Structured PDMS sheets can easily be bonded to a glass plate or another sheet of polymer owing to its excellent adhesion properties. For a non-permanent bond for low-pressure applications,

22

the PDMS sheet can simply be pressed against the closing sheet and makes conformal contact with that surface. Consequently, the relief structure in the mold forms a network of empty channels. A low-viscosity liquid pre-polymer is placed at the open ends of the network of channels; then by capillary action the liquid spontaneously fills the channels due to the pressure difference between the two hydraulically connected regions of the liquid mass.

After the pre-polymer solution accepted the shape of the PDMS patterns, it was photopolymerized, "In-situ". 16.5 wt% NIPAAm, 0.4 wt% BIS, and 0.005 wt% of microspheres were dissolved in isopropanol. The solution was then bubbled for 20 minutes in order to remove the remaining oxygen. Photopolymerization was then initiated by adding 0.16 wt% of DMPA and using an uncollimated, 365 nm, 300 mW/cm^2 light source (EFOS Ultracure 100ss Plus, UV spot lamp, Mississauga, Ontario) under an inert nitrogen environment for 8 minutes. Finally, after filling the channels and photo polymerizing the prepolymer into a solid, the PDMS mold is removed, and a network of poly(NIPAAm) remains on the surface of the substrate.

The formation of hydrogel microstructures was based upon the UV initiated free-radical polymerization of the acrylate end groups in NIPAAm. The radical polymerization begins by the dissociation of DMPA upon exposure to the UV radiation. This creates highly reactive methyl radicals, which then attack unsaturated carbon-carbon double bonds (C=C) of acrylate functionalities on the macromer. Since two reactive centers per macromer are created, propagation

23

results in the formation of a highly cross-linked polyacrylate network. This network represents a three-dimensional structure capable of entrapping the fluorescent microspheres.

It should be stated that the C=C conversion cannot be completely correlated to polymerization in the gels because of the presence of oxygen during illumination. A fraction of acrylate groups will be converted to oxygenated species rather than participate in the polymerization process due to the reaction of oxygen with radicals formed in the gel which effectively terminates propagation.

In addition, the surface of the coverslip will also participate in the free-radical polymerization reaction due to the unsaturated C=C functionalities from the TPM monolayer. Methacrylate groups on the surface of the substrate react with radical species present near the surface to effectively anchor the gel to the surface of the substrate.[16] Thus, delamination or detachment of poly(NIPAAm) networks from the substrate did not occur, even though extensive swelling did occur in the gels upon exposure to water.

Filling up of the channels and subsequent polymerization of the pre polymer solution does have several limitations. First, it requires a hydraulically connected network of capillaries; it cannot, therefore, form isolated structures or patterns on contoured surfaces. Also, although capillary filling over a short distance (ca. 1 cm) can be achieved quickly and efficiently, the rate of filling over

24

a large distance decreases significantly due to the viscous drag of the fluid in the capillary. Moreover, the forward ends of capillaries may fill incompletely if the hydraulic drag is sufficiently high.[43] Interestingly, capillaries with closed ends may fill completely if they are short; the gas in them appears to escape by diffusing into the PDMS.[12] In addition, even though there is large amount of solvent in the polymer solution, the solvent can be easily evaporated at room temperature since both sides of the channels are open. Therefore, the solution should be polymerized immediately after the channels are completely filled, which occurs relatively fast [44] in the cross-sectional sections used for this report. Lastly, a PDMS structure theoretically could be reused after being peeled off the coverslip; in practice, however, the surfaces are likely to be contaminated and a second sealing does not hold tight.

2.5.   Fabrication of Fluidic Chamber

The fluidic chamber was constructed by sealing a 2 cm (diameter) rubber ring between a no. 1 cover slide and a 3" x 1" plexi glass sheet. In addition, several 5 mm (diameter) rings were sealed in the corners of the cover slide with nail varnish in order to give more rigidity to the structure (see Figure 2-7, Figure 2-8, Figure 2-9).

25

2.6. Remarks

Due to mechanical forces associated with volume changes in the gel during water induced swelling, the poly(NIPAAm) microstructures easily detached from surfaces not treated with TPM. However, hydrogel structures fabricated on TPM treated glass substrates did not show an increase in diameter at the base of the structures because they were covalently fixed to the substrate surface. Nonetheless, poly(NIPAAm) array elements became swollen and increased in height by nearly 30% - 50%. Height changes of 32% and 51% were observed for gel microstructures made from 5 um and 25 um PDMS molds, respectively. Such behavior is expected because surface anchoring of the gel prevents the hydrogel array elements from swelling laterally at their base but does not inhibit swelling upward.
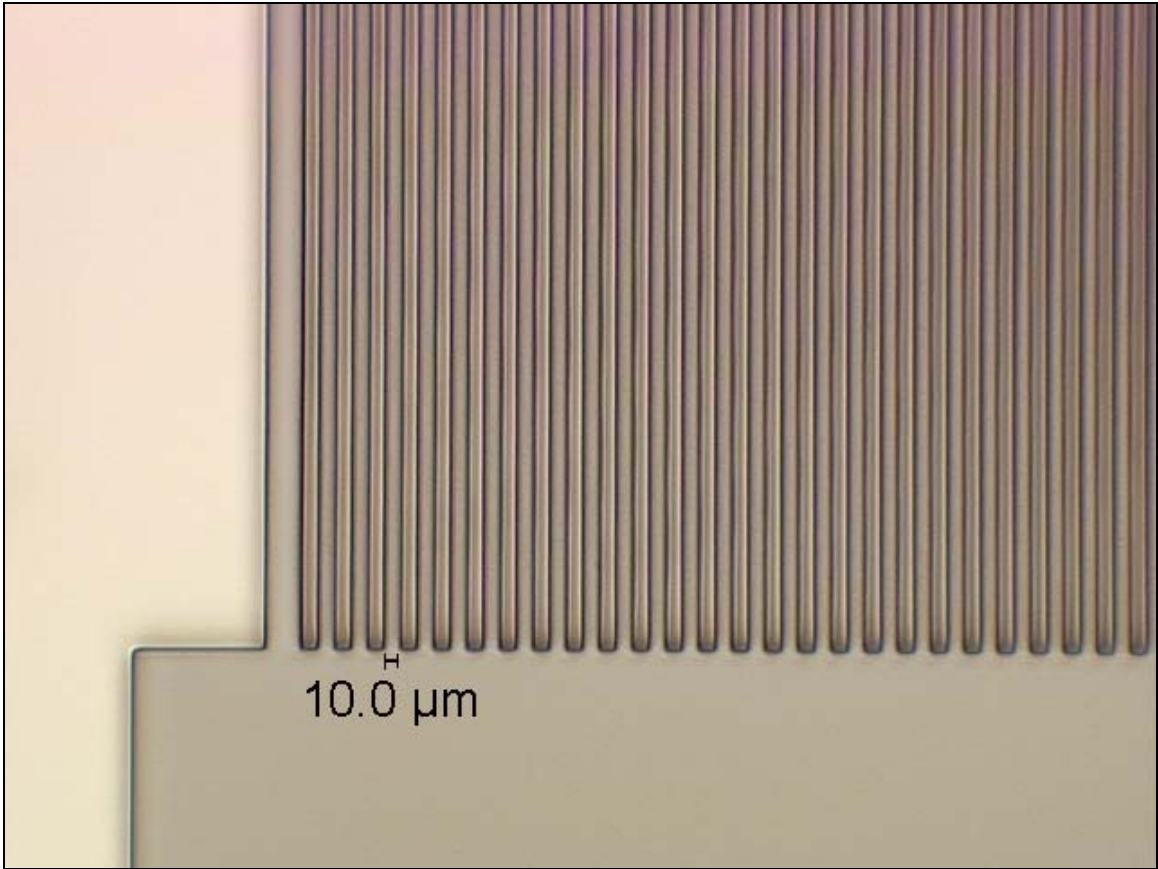
Figure 2-1. SU-8 microstructure
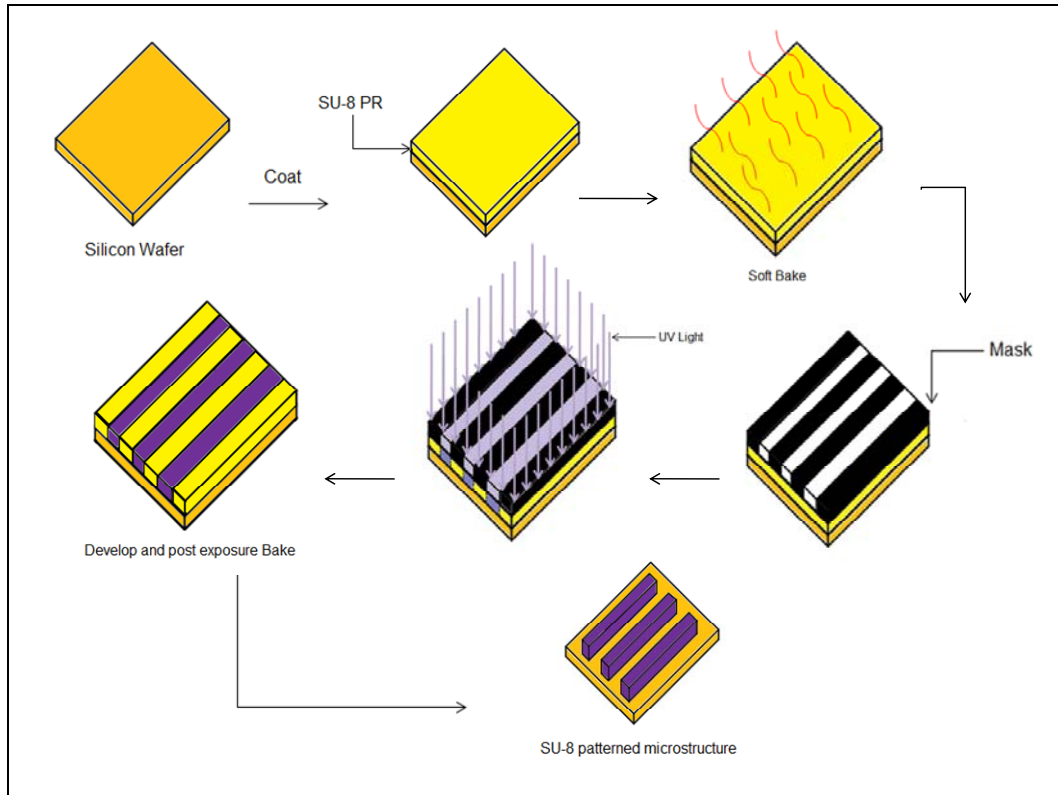
Figure 2-2. Development of SU-8 master molds by photolithography
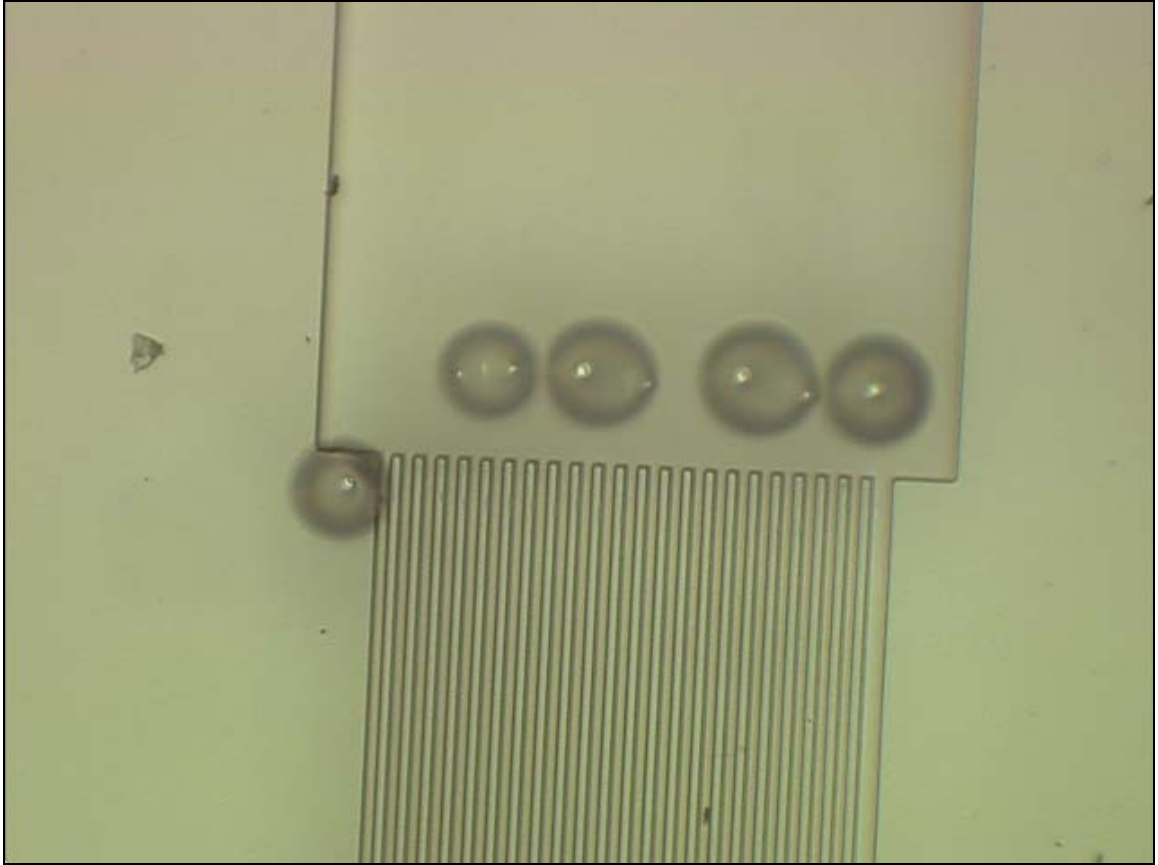
Figure 2-3. PDMS mold with bubbles
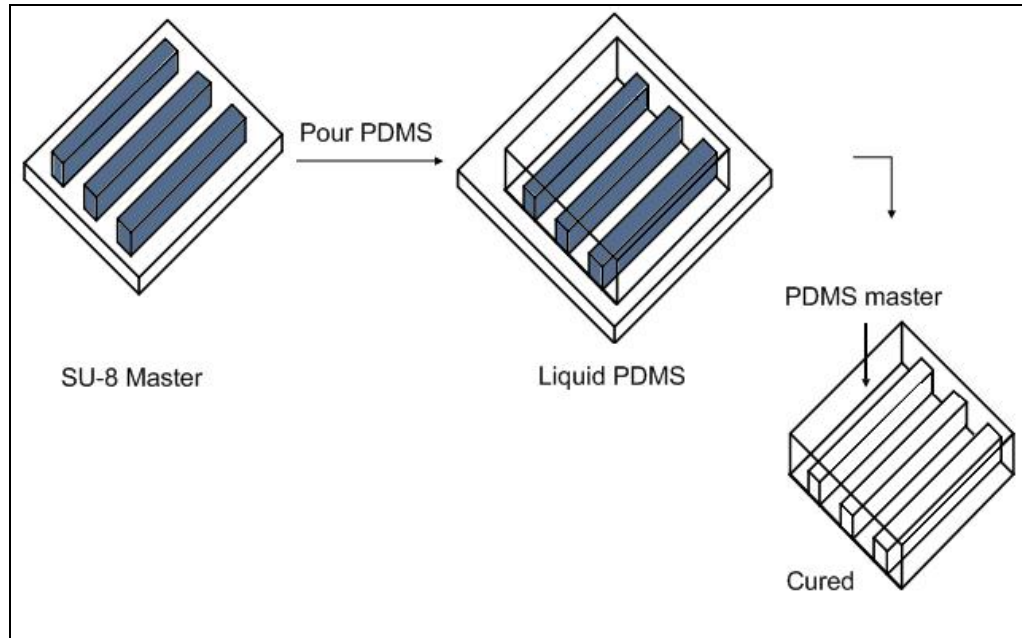
Figure 2-4. Fabrication of PDMS molds
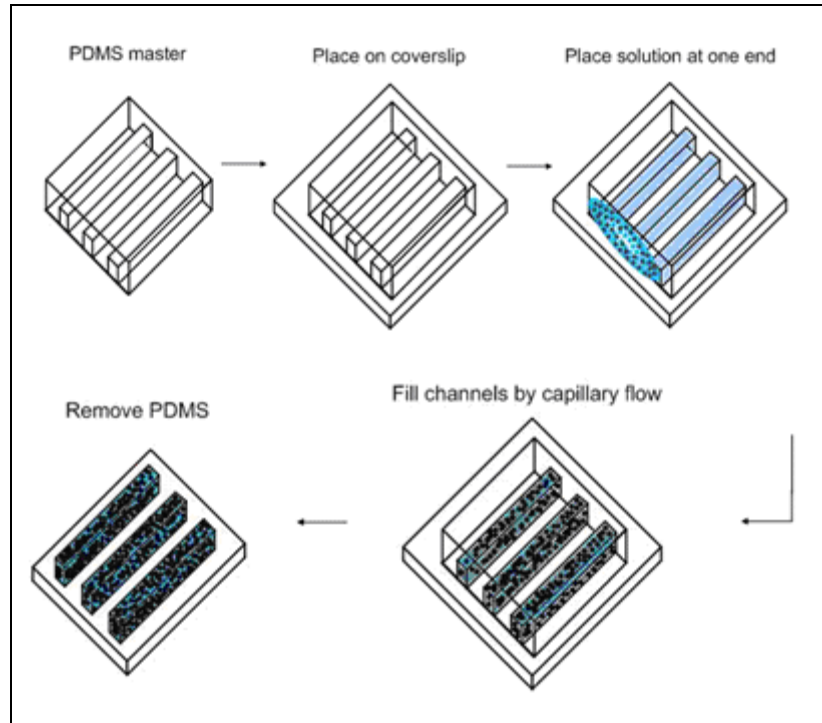
Figure 2-5. Processing for poly(NIPAAm) patterning

31
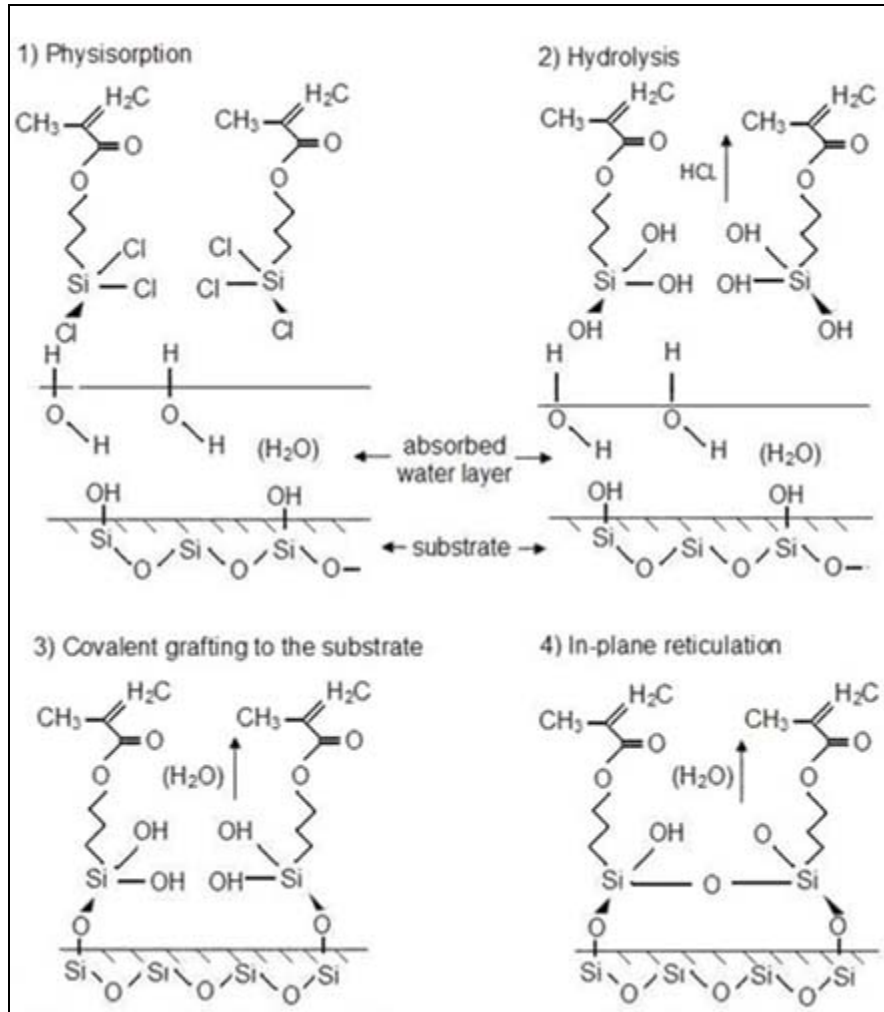
Figure 2-6. Silanization mechanism of glass surfaces by using a monolayer of 3-(trichlorosilyl)propyl methacrylate (TPM)
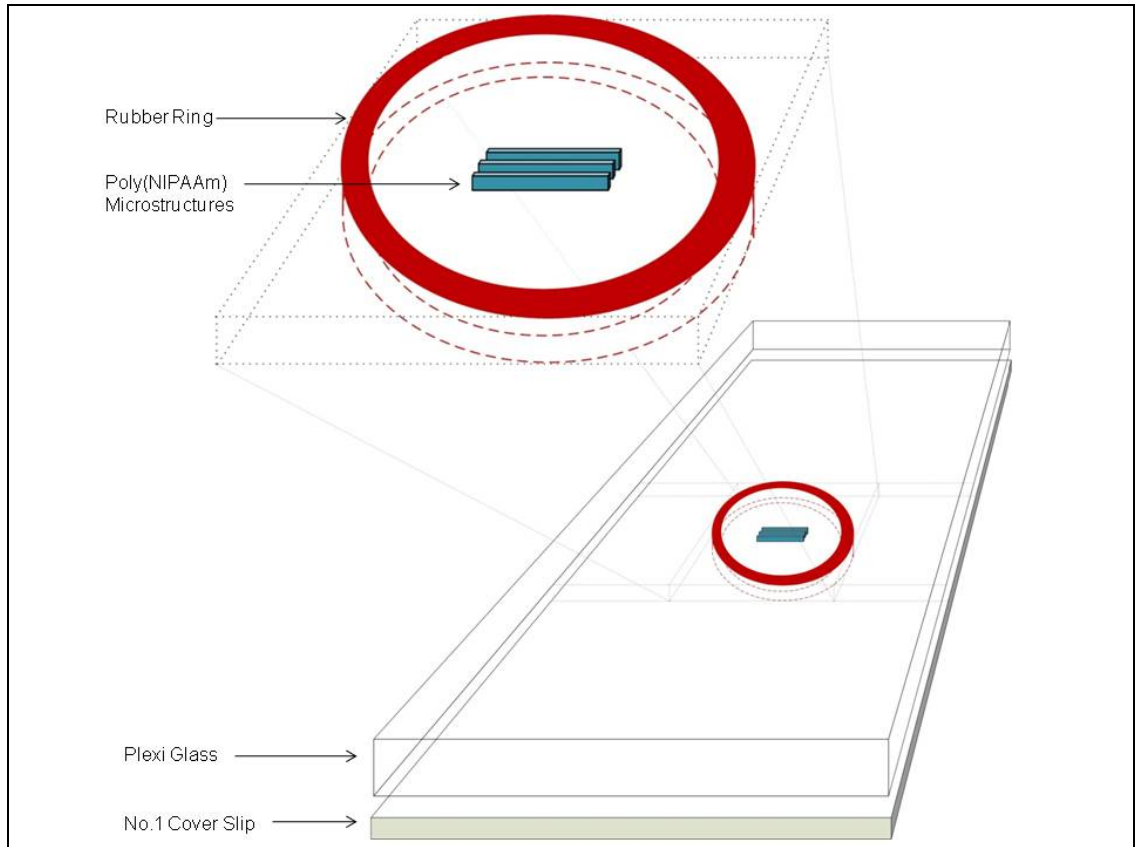
Figure 2-7. Fluidic chamber in 3D
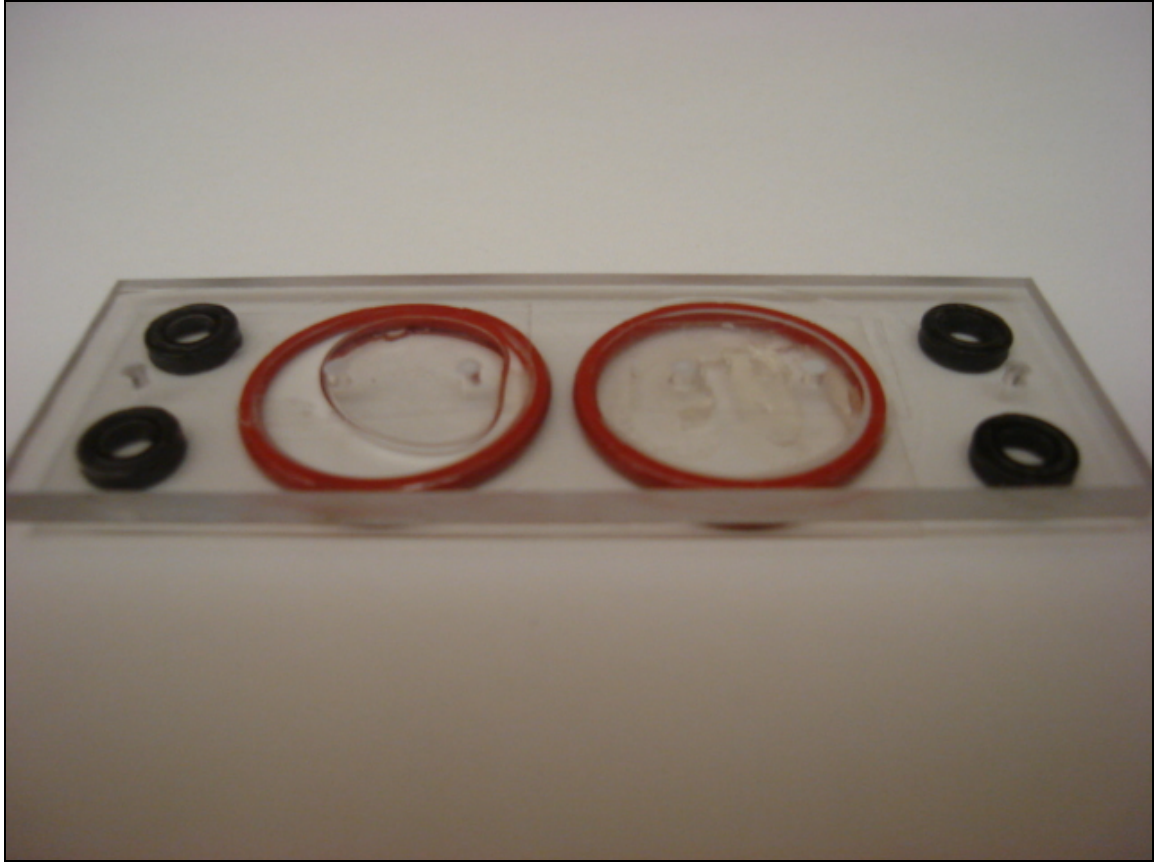
Figure 2-8. Front view fluidic chamber

Figure 2-9. Side view of fluidic chamber

CHAPTER THREE: CHARACTERIZATION OF SWELLING OF HYDROGELS BY SPINNING DISK CONFOCAL MICROSCOPY

3.1. Introduction

Optical microscopy is a technique that is widely used in many systems when investigating the sub micrometer to micrometer range. When light enters dense samples, such as biological tissue, it goes through many scattering events, which can leave the image blurry, thus making it difficult for deep visualization within the sample. Marvin Minsky faced this very significant problem in the 1950's. He was looking for a way to visualize the nervous system, and the nerve cells connected to it. He developed a two-step solution. The first step was reducing aberrant rays of scattered light from around the target point of interest. This was accomplished by using point by point illumination of the sample. The second step was to take a pinhole-sized opening in the image plane on the other side of the objective, which was used to eliminate out-of-focus light. This prototype for the first confocal microscope used a carbon-arc lamp as the light source and a translating stage to visualize each point of the sample. Other subsequent improvements use a method of scanning the laser beam

36

instead of translating the sample. These two processes helped establish confocal

microscopy as a powerful tool in various scientific fields.[45]

3.2. Confocal Microscopy Introduction

As conventional optical microscopes use a halogen lamp and other

surface light sources, diffused light from places other than the point of interest

are mixed with the light from the point of interest. Moreover, when planar photo

detectors like cameras or eyes are used, blurred, out-of-focus light from the

points shifted toward the optical axis are observed, overlap with the observed

light. For these reasons, the conventional optical microscope has a limited spatial

resolution.[46] On the contrary, confocal microscope systems use laser beams to

illuminate samples with pin-point accuracy, to eliminate diffused light from

sources other than the point of interest. In addition, pin-hole windows are

provided in front of the light detector to cut off light from sources other than the

point of interest for high resolution (see Figure 3-1).

3.2.1. Advantages of Confocal Microscopy

There are several advantages of using confocal microscopy rather than

electron microscopy and conventional light. First, the confocal microscope

visually divides the images into sections (see Figure 3-2 and Figure 3-3). In

37

doing so, it reduces any problematic areas that would otherwise be observed using electron microscopic techniques and conventional light. Also, both living and fixed samples can be viewed with greater precision since optical sectioning is generally noninvasive. In addition, information can be collected from a well-defined plane instead of from the entire sample thickness due to the shallow depth of field of the optical sections (see Figure 3-4). As a result, the image is black since it is no longer collecting light that is out of focus when the focal plane is above or below the specimen. By reducing the light that is out of focus, this improves the clarity, contrast, and detection sensitivity. Figure 3-5 shows the comparison between confocal and conventional light microscope when the object lens is focused well below the fluorescent sample.

Another advantage of confocal microscopy is vertical sectioning. By taking optical sections in different planes, cells are scanned both laterally as well as in depth. The optical sections can also be obtained digitally, which is beneficial because the prints can be done quickly, as opposed to using darkroom materials, which take longer to develop.

3.2.2. Disadvantages of Confocal Microscopy

Unlike the conventional fluorescence light microscope, confocal microscopes are limited by the available wavelengths of light that are produced

www.manaraa.com

by laser lines. If the laser light has not been properly attenuated, the intensity of the beam could be harmful to living cells.

Price is another issue to consider when using a confocal microscope. Depending on the one used, they can cost over ten times more than a typical conventional fluorescence light microscope. However, this can be remedied if shared among researchers in a centralized facility. This is especially beneficial when taking into account the size of the microscope. A confocal microscope takes up more space than a conventional fluorescence light microscope since it needs more space for computer hardware, a laser, and scan head.

3.3.   Spinning Disk Confocal Microscopy Introduction

One type of confocal microscope uses a spinning Nipkow disk, a stationary light source, and a stage. The Nipkow disk, which is used to raster scan the sample, is a black, metallic-coated, glass disk that has various openings 20-60 um in diameter. They are arranged in an interlacing pattern. Figure 3-6 depicts the pattern arrangement of the Nipkow disk. One of the special features of this microscope is that specimens can be viewed directly in their true colors as a confocal image in the reflected as well as the fluorescence mode. Since the disk can spin at speeds of up to 3600 rpm, the images can be viewed in real time, which allows direct confocal focusing through the sample (see Figure 3-7).

39

Spinning disk confocal microscopes scan the specimen with thousands of spots of light concurrently, as opposed to CLSMs, which use one spot of light to scan the specimen (see Figure 3-8 which illustrates this difference). Light from each spot traces a single scan over successive parts of the specimens. Spinning disk confocal microscopes are also different from CLSMs: instead of using coherent laser light to scan the specimen, a broad-spectrum, white light is the illumination source as in conventional light and fluorescence microscopy. The white light source can either be mercury or xenon, allowing for the selection of any filter combination employed for conventional epifluorescence. Dyes excited by UV can be imaged confocally along with fluorescein, rhodamine, and infrared dyes without the added expense of UV and infrared lasers. Cells that are labeled with multiple fluorochromes can therefore be imaged confocally in their true colors. Some spinning disk systems use laser light for fluorochrome excitation. The design of spinning disk confocal microscopes is also different from the CLSMs in that only x y sectioning is possible. Another noteworthy difference from CLSMs is that a computer is not needed for most spinning disk confocal microscopes to work.

In older spinning disk systems, the Nipkow disk typically transmitted only 1% of the illumination, resulting in dim fluorescence images. Unless fluorescent samples were bright, an intensifying video camera or cooled CCD camera was needed to generate sufficient signals and improve the signal-to-noise ratio. The relatively large size (60 μm) of the confocal apertures in the Nipkow disk, as

compared to CLSMs compromised optical sectioning so that optical section thickness was approximately 1 µm for spinning disk confocal microscopes as compared to 0.5 µm for CLSMs with the same objective. Newer models of confocal microscopes have addressed the lack of brightness using microlenses. There are two types of spinning disk confocal microscopes: the tandem scanning (not included in this thesis) and monoscanning microscopes.

3.3.1. Mono Scanning Confocal Microscopy Introduction

The monoscanning spinning disk confocal microscope (see Figure 3-9) also uses a spinning Niplow disk with spirally arranged openings. It uses non-coherent white light for illumination, and produces real time images. This microscope detects light through the same aperture from which a given area of the sample was illuminated. Therefore, illumination and imaging are performed at the same time using the same aperture, which allows for easier alignment of the Nipkow disk. To reduce unwanted light reflected by the Nipkow disk, one version of the confocal microscope, the K2-S Bio, tilts the Nipkow disk and uses polarized light.

Newer models of the monoscanning confocal microscope use a second disk which has 20,000 microlenses that are aligned and spin together with the apertures in the Nipkow disk, unlike older models, which suffered from loss of light. This amplifies the light transmitted to and from the Nipkow disk.

41

Furthermore, background light in the microscope that was developed by the Yokogawa Electric Company is reduced since the dichroic mirror is positioned between the Nipkow disk and the disk containing the microlens array. Confocal microscopes using the microlense array have been used to examine microcirculatory events and calcium ion dynamics.

Finally, the data shown in this report is obtain from the Perkin Elmer Ultra View confocal microscope system, which is an updated version of the Yokogawa unit that employs dual spinning disks with microlens technology together with either argon ion or krypton-argon ion laser, and digital cooled CCD camera detection to produce images. Both fast and slow scan rates are available. Fast temporal data acquisition with frame transfer or interline cameras at 12 or 14 bits per pixel lets images be captured at video rates or faster (50 frames/s and as fast as 120 frames/s). This is especially useful for imaging ionic fluctuations in living cells and tissues.

3.3.1.1. Operation of the Dual-Spinning Disk Confocal Microscope

Please refer to Figure 3-7 for an illustration of the system. The expanded and collimated laser beam illuminates the upper Nipkow disk containing roughly about 20,000 microlenses. Each microlens focuses the beam onto the corresponding pinhole. In doing so, it significantly raises the fraction of the illuminating beam that is transmitted by the main Nipkow disk containing the

42

pinhole array. The beams then go down to fill the opening of the objective lens. The objective lens produces a reduced image of the pinholes into the sample focal plane. Fluorescence is captured by the objective lens exit pinhole and eliminates fluorescence from out-of-focus regions, and thus transmits fluorescence that started from the sample region illuminated by that particular pinhole. On the other hand, for samples that have fluorescence distributed over large depths, some out-of-focus fluorescence can escape through nearby pinholes in multiple pinhole systems. The rays sent out by the exit pinholes are averted by the dichromatic beam splitter, which is between the two Nipkow disks, and go on to the image plane.

The principle of operation of the - dual-spinning-disk confocal is described in detail elsewhere.[47] Briefly, in the Ultraview unit, the light input from the fiber goes through some beam-shaping optics and is delivered onto a disk spinning at 1800 rpm. The disk contains a helical array of 20,000 microlenses spaced at 250-µm center-to-center distance which collect the light and each creates a scanning laser point source as the disk spins. The point sources pass through a reverse multibandpass dichromatic mirror (Chroma, Brattleboro VT) (see Figure 3-10 for an explanation of the dichromatic mirror) and through a Nipkow disk spinning at the same rate and containing 50-µm pinholes positioned precisely conjugate to the microlenses. The scanning point sources leave the confocal head and enter the inverted microscope via a c-mount-coupled side camera port and are focused onto the specimen through the objective lens. Fluorescence

43

emission from the specimen is then collected by the objective, and out-of-focus emission is removed in the Ultraview unit by the spinning Nipkow confocal pinhole array. The focused emission that passes through the pinholes is reflected by the reverse dichromatic mirror away from the microlenses, through a multibandpass emission filter, and to the camera.[48]

3.3.1.2. Advantages of the Dual-Spinning Disk Confocal Microscope

The dual-spinning-disk system has important advantages over both the laser scanning confocal microscopes, as well as traditional single Nipkow disk confocals. First, the pinhole array on the Nipkow disk of the Ultraview is made to scan twelve image frames per rotation, which are 360 frames per second. The laser scanning confocal, on the other hand, only does ~1 frame per second. Also, multiple point sources scanning the specimen gives "real-time" confocal imaging, which allows one to see a full confocal image through both the ocular as well as on a camera. On the other hand, in a single scanning beam in a laser-scanning confocal, the entire sample must be registered serially, which makes low-noise CCD detection impossible, and leaves it to be limited to noisy photomultiplier tube detectors, which are unsuitable for FSM. It is also important to note that in traditional Nipkow disk confocals, only about 5% of the incident illumination makes it through the pinholes to scan the specimen. However, the microlenses in the Ultraview amplifies the illumination efficiency to theoretically

44

~40%.[46] The positioning of the reverse dichromatic mirror between the two spinning disks stops the emission from the specimen from being defocused by the microlenses in the upper disk.[48]

For multispectral imaging by the confocal, a dual-bandpass reverse dichromatic mirror is used, as well as an emission filter set for the 488 nm ex/525 em and 568 ex/605 em (Chroma). Various other filter sets are now available from Chroma, including dual sets for excitation at 442/514 and 457/514, and a triple set for 488/568/647. It is important to note that reverse dichroics are complicated and not easy to manufacture. Also, the ones made for this application are on a very specialized substrate so as to not misalign light coming from the microlenses as it goes through the pinholes, making them very expensive.[48]

3.4.   Image Processing and 3D Rendering of Stacks

3.4.1. Three-dimensional Image Processing

Since the scanning-disk confocal microscope is used directly for the non-invasive serial optical sectioning, yielding high resolution images free from out-of-focus blur, it permits the direct acquisition and study of complete in-focus 3D data sets.

Once a series of images has been collected, the 3D data set, which these comprise, may be manipulated in many ways. A great advantage of this technique is that optical sections are already in spatial register, and thus do not require computational alignment before subsequent processing.

The availability of high resolution non-overlapping optical section series makes it possible to undertake the accurate quantization of structural features in the sample, using a variety of unbiased estimators for 3D stereological analysis, ImageJ. In addition, there exists a wide variety of image processing and analysis procedures that can be applied to further enhance the images, or to extract features for subsequent measurements or display.

Confocal images, for all their advantages, are not perfect, and it is possible to enhance them further by subsequent computational image restoration processing to remove residual blurring due to the 3D point spread function of the confocal system.

3.4.2. Surface and Volume Rendering

By making use of surface rendering procedures that are standard on graphics work stations, compact fluorescent objects can be displayed as surface shadowed or surface luminant.[45] In other words, 3D rendering methods convert 3D data sets into 2D pictures, or a sequence of 2D pictures, in order to provide

interpretation of the 3D structure. Among a multitude of possible projection methods are the summed-intensity, maximum-value, voxel-gradient shading and alpha blending. The maximum-intensity projection is demonstrated in this thesis.

For more complex procedures, the primary problem relies on the defining of the object surface required for these procedures from the original unsegmented 3D voxel image, using some kind of threshold algorithm; ImageJ standard threshold algorithm was used for the processed images shown in this work. Once the voxels are defined by identifying the surface of the object to be displayed, e.g. microspheres, the other voxels of the image are discarded, to produce a very much smaller data set which can be handled easily by the workstation. More sophisticated volume rendering algorithms allow altering of the constants that model transparency or reflectivity, so that the rendered objects can be displayed as opaque or semi-transparent. For instance, it will be possible to see structures within other structures, such as the microspheres within poly(NIPAAm) trenches.

3.4.3. 3D and 4D Animation of Confocal Images

The ultimate development of confocal images display is to compute not just a single stack of images forming a 3D structure, but time incremental series of such stacks that may subsequently be displayed as an animation sequence. This 4D animation displayed may be achieved by storing the complete animation

47

sequence of two time points at any one time, the first being overwritten from the disc by that for the time point-after-next while the second is being displayed. Such a four-dimensional (x, y, z, t) display of a time-lapse series of confocal images collected from a 3D structure enables one to study phenomena such as hydrogel dynamics. However, the amount of memory required for the storage and displayed of pre-computed animation sequences is vast. Therefore, special graphic workstations should be use. A fellow group member is investigating the expediency of such methods to analyze the buckling of patterned poly(NIPAAm) hydrogels (unpublished data).

3.4.4. Fluorescence Images of Fluorescent Microspheres

To investigate the local swelling of poly(NIPAAm) microstructures attach to pendant surfaces, fluorescent microspheres were embedded into the polymer solution. The fluorescence microspheres are optimally excited at 468 nm, with an emission maximum at 508 nm. Figure 3-11 (A) shows a fluorescent micrograph of the patterned poly(NIPAAm) above the LCST. Figure 3-11 (A) is the original image and Figure 3-11 (B) is after wavelet application. Figure 3-11 (A) and Figure 3-11 (B) demonstrate the capability of the wavelet analysis to select features of interest in the bead data and to reduce background. In both figures 15% threshold is set relative to the maximum in each image. Therefore, the lower 15% intensity pixels are blanked out. As you can see, in Figure 3-11 (A), the

48

broad background fluorescence (with low spatial frequencies) has been subtracted by the wavelet application. This is a convenient way to automatically select objects with certain morphologies in an image for further analysis. For instance, the fluorescence information can then be fitted only from the bead locations selected by the wavelet application. In further sections, the practicality of such an application to analyze automatically large sets of data is highly useful.

3.5. Image Processing Routines to Locate Particle Positions in Three Dimensions

Real-space images are collected with a spinning-disk confocal microscope. Images sizes are 6.45 μm in the x- and y-directions. Image stacks typically contain approximately 150 - 400 images, each offset by 0.05 – 0.15 μm in the z-direction. Fluorescence is excited using with the 488 nm line of an Ar+ ion gas laser; the fluorescence is filtered with a 500 nm long-pass filter, and is detected with a photomultiplier tube.

Images are analyzed using image processing routines to filter the images and locate particle positions in three dimensions. Images with the computer-determined particle positions overlaid are routinely checked to ensure accuracy. All the image processing data acquire for this thesis was obtained using ImageJ which is a public domain, Java-based image processing program developed at the National Institutes of Health, ImageJ.

49

The procedure in the location of the particles positions involved background subtraction and Gaussian filtering of the images and location of the particle centers in 3D based on regional intensity maxima. Subsequently, the locations of the centers were refined to subpixel accuracy based on moments of the local intensity distribution. Once the location of the centers was obtained a Matlab routine was used in the reconstruction of 3D geometric figures using Delaunay triangulation procedures. Delaunay triangulation is a triangulation such that no point in a set of P points is inside the circum-hypersphere of any simplex in a triangulation DT(P). In other words, it is a set of lines connecting each point to its natural neighbors. The Delaunay triangulation is related to the Voronoi diagram which is a special kind of decomposition of a metric space determined by distances to a specified discrete set of objects in the space. The use of Delaunay triangulations is particularly suited when we do not want to force any constraints on the set of points to be connected.

By means of Delaunay triangulations, we directly quantify the local spatial structure of the surface-attached hydrogels by measuring the distribution of the microspheres inside the polymer.
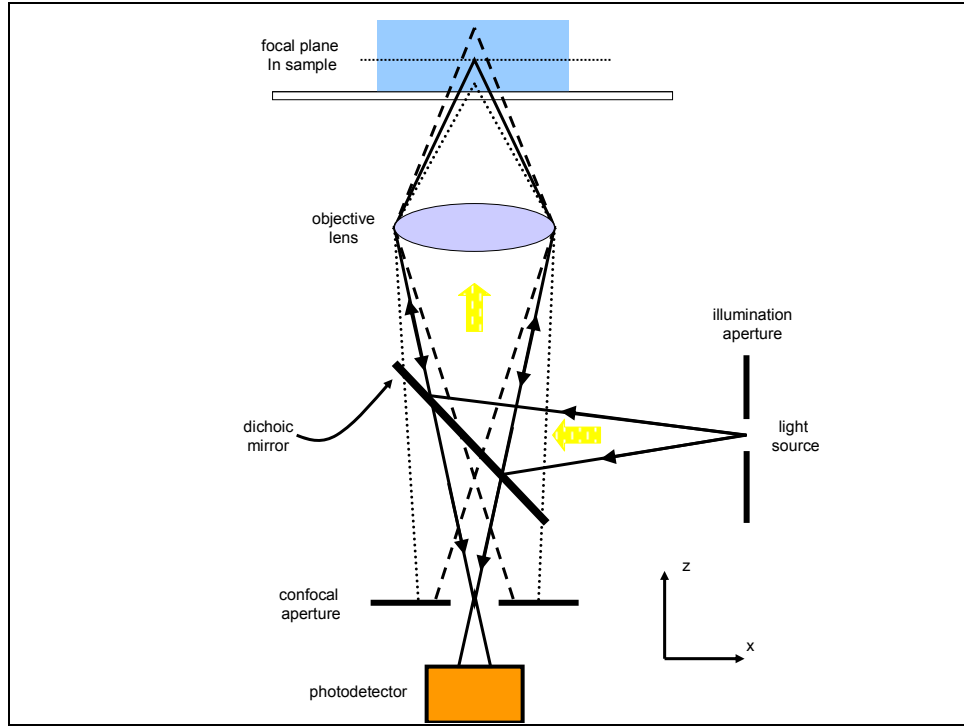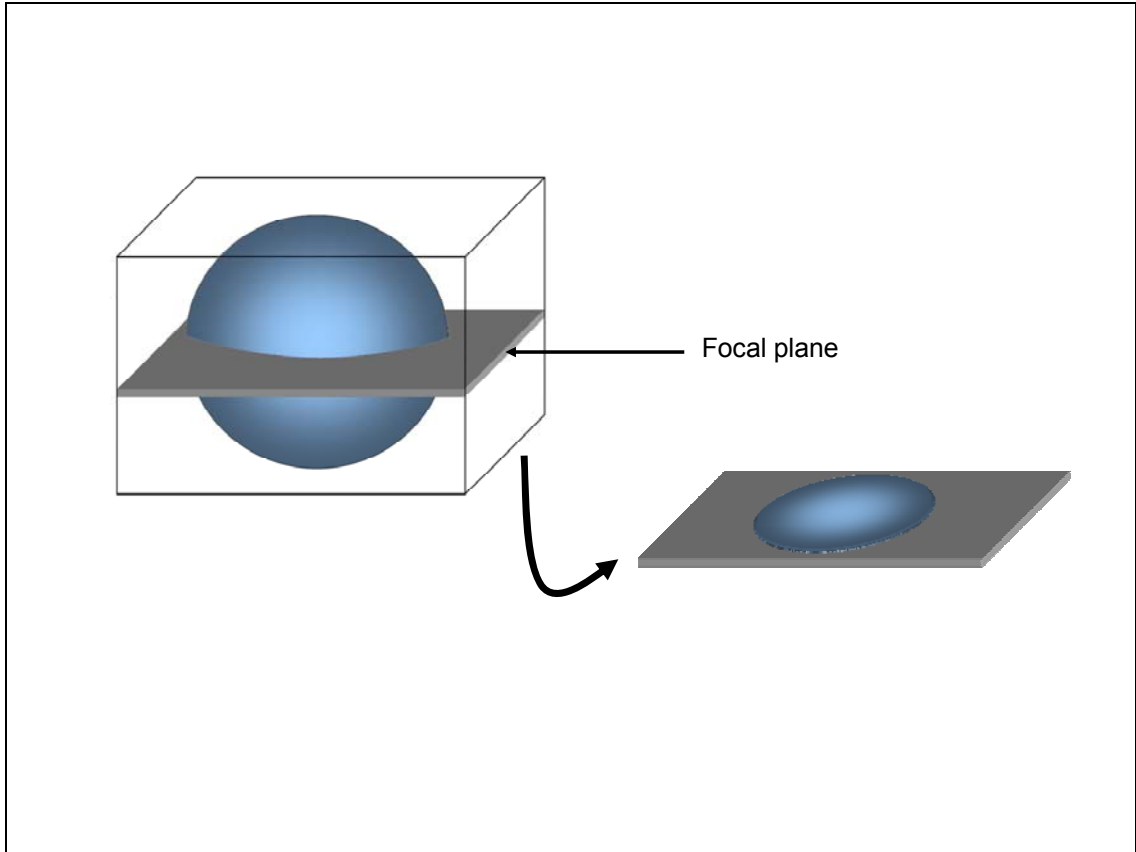
Figure 3-1. Schematic diagram of the confocal microscope principle
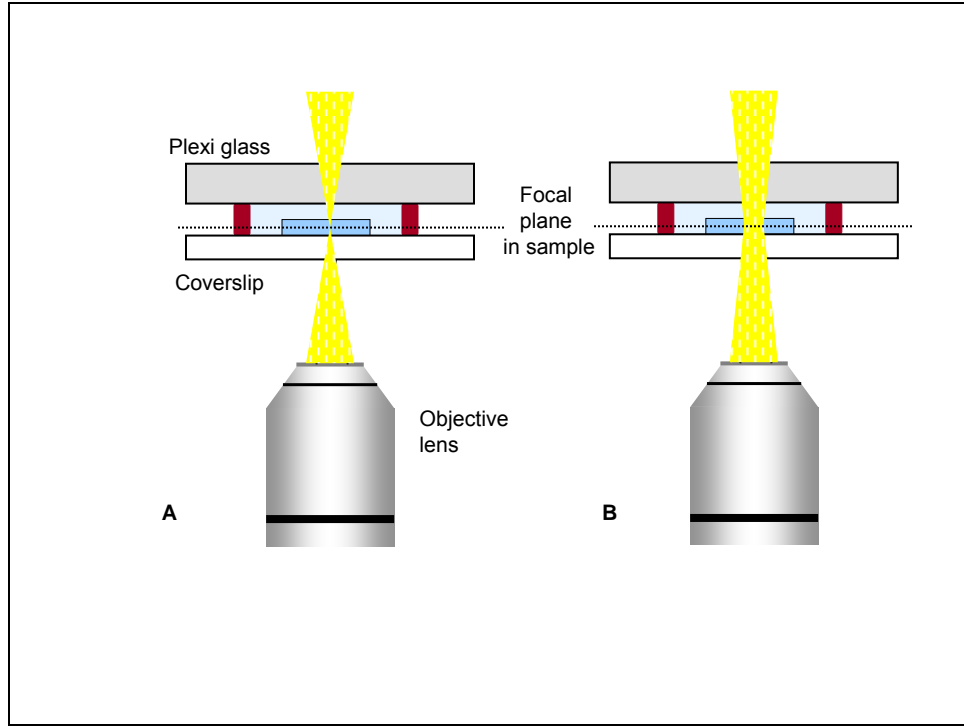
51
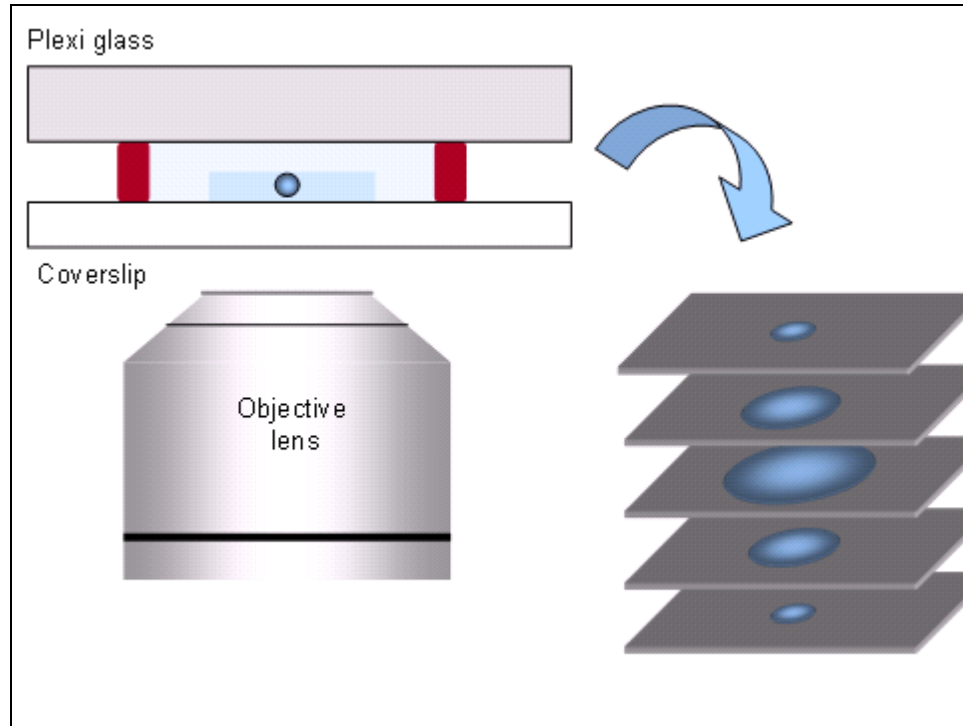
Figure 3-2. Schematic diagram demonstrating the principle of optical sectioning
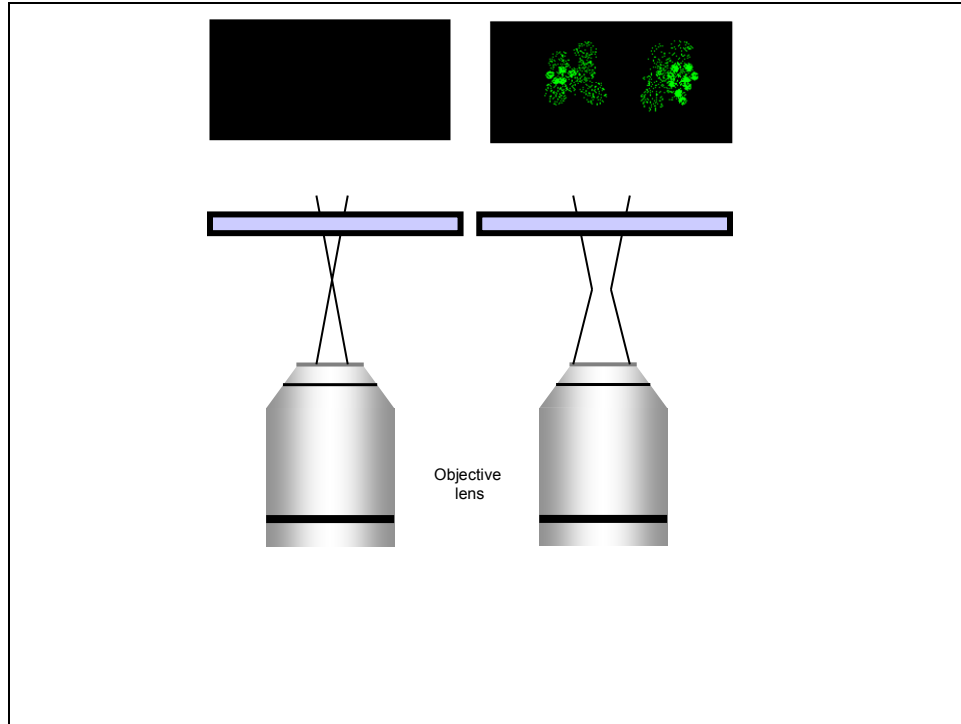
Figure 3-3. Diagram showing generation of optical sections in the confocal microscope

53

Figure 3-4. Comparison of specimen illumination in confocal (A) and conventional (B) microscopes

Figure 3-5. Comparison of confocal and conventional light microscope when the object lens is focused well below the fluorescent sample, depicted by the small rectangular box
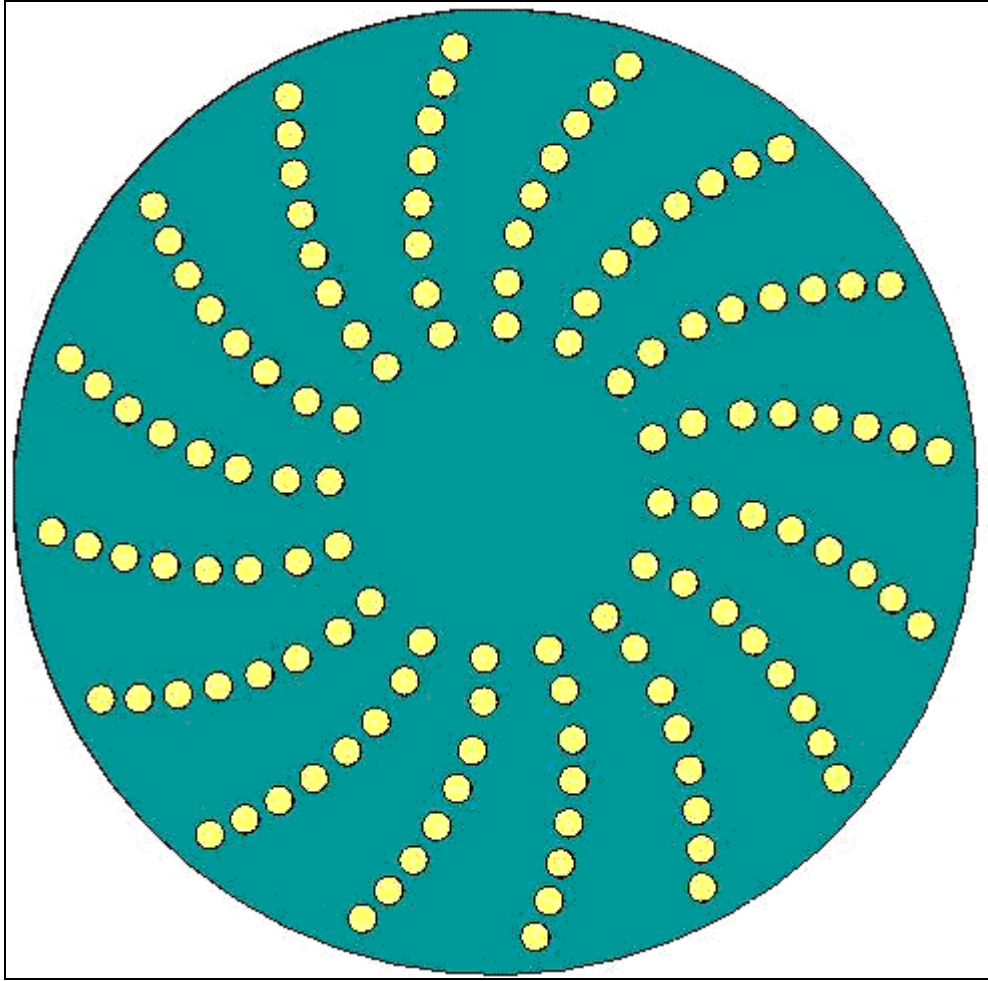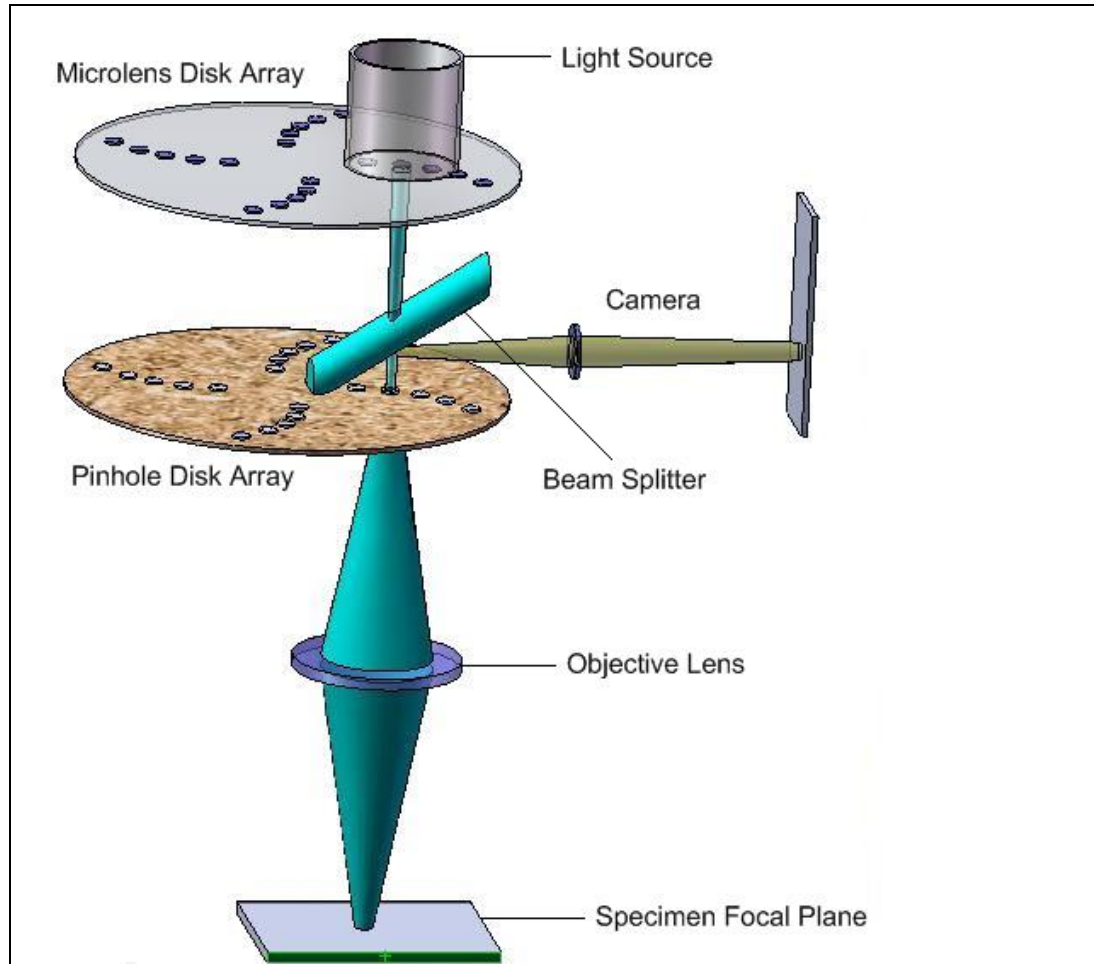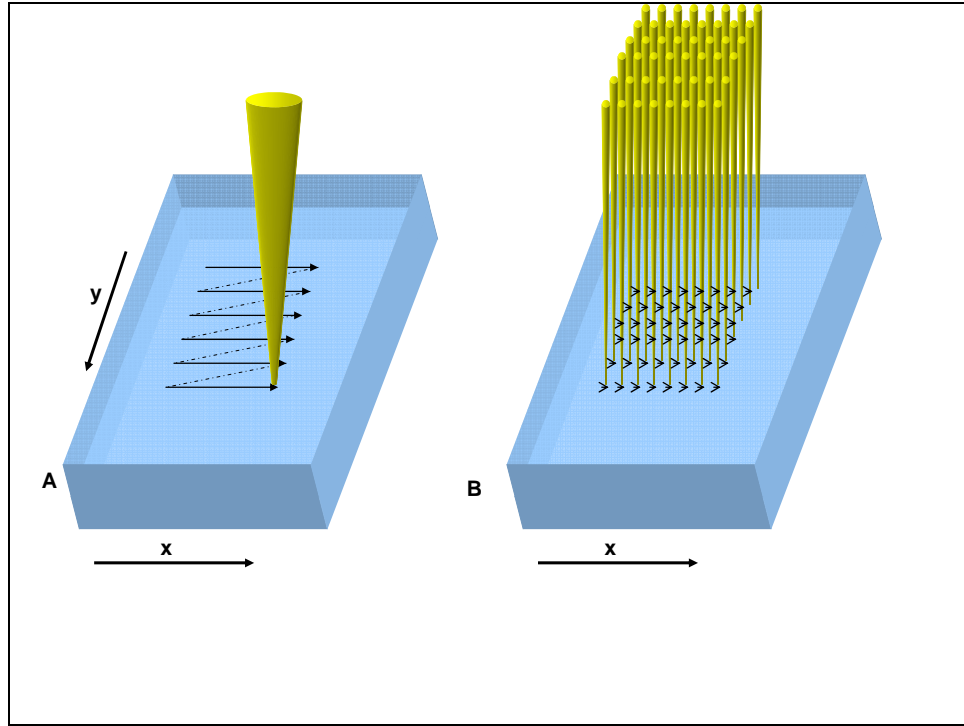
Figure 3-6. Nipkow disk

Figure 3-7. Spinning-disk confocal microscope

Figure 3-8. The raster scan pattern that (A) confocal laser scanning microscopes and (B) spinning-disk confocal microscopy commonly use to generate images

58
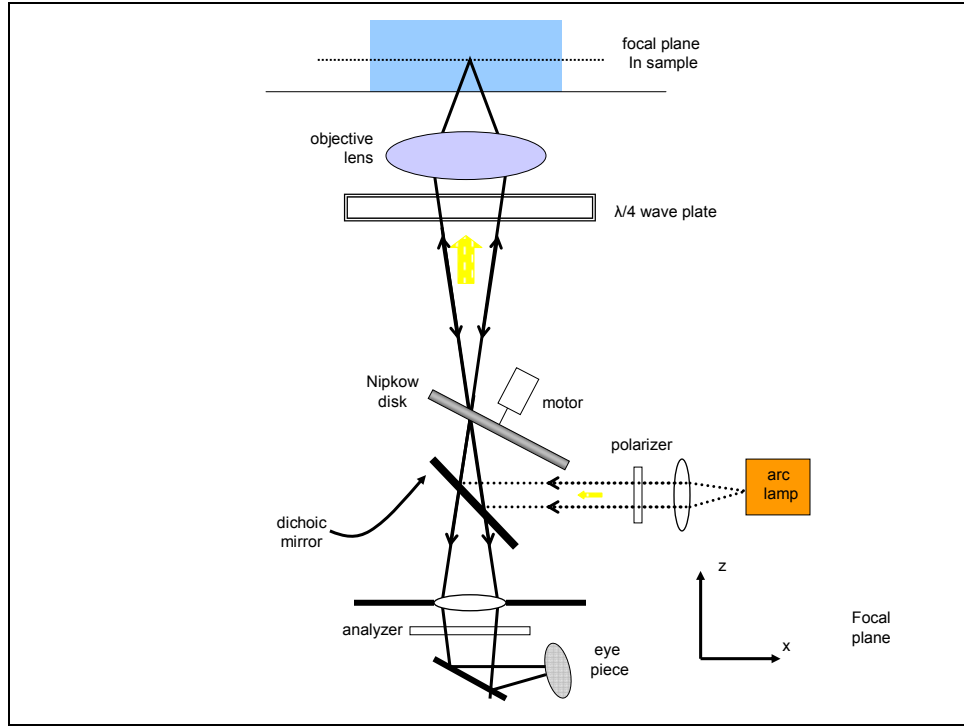
Figure 3-9. Schematic diagram of the optical path in a monoscanning confocal microscope

59
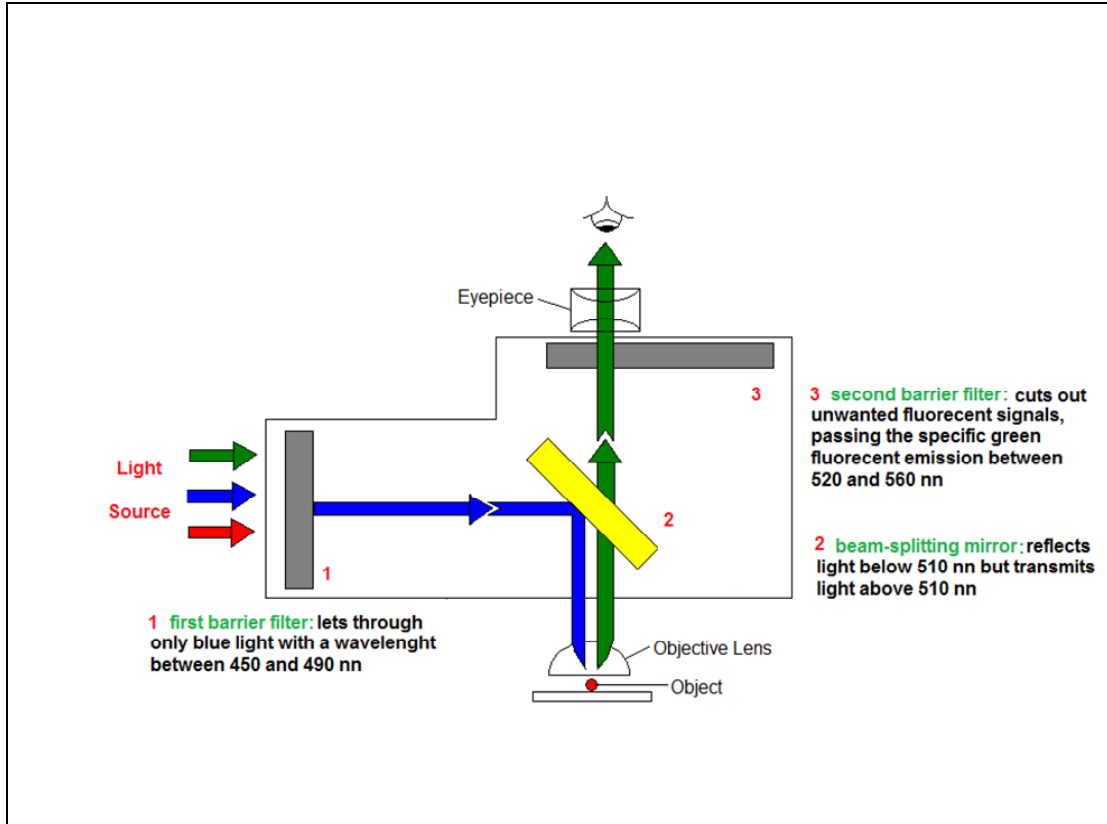
Figure 3-10. Epifluorescence microscope principle

Figure 3-11. Background subtraction using the wavelength of the fluorescence microspheres

61

CHAPTER FOUR: RESULTS, DISCUSSION, AND CONCLUSIONS

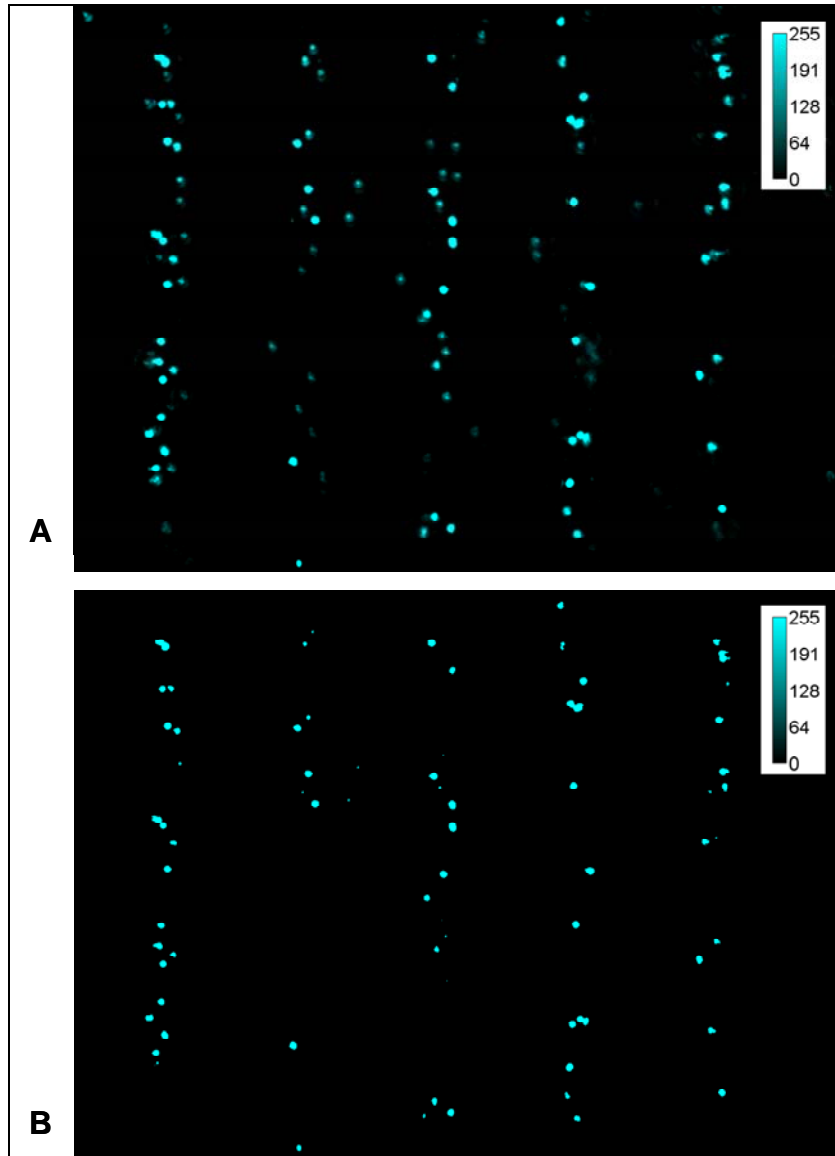As stated in Chapter One, the study reported here examined in detail the techniques used for the fabrication of poly(NIPAAm) microstructures on silane coated surfaces. These techniques required the overcoming of several challenges that will be address in this section. In addition, the successful attachment of the polymer networks to the glass surface will be illustrated with spinning-disk confocal microscopy images. Furthermore, the swelling and des-swelling (Figure 4-1, shows a cross-sectional section of the trenches in the collapse state); the buckling and un-buckling effect of the polymer trenches (see Figure 4-2) will be analyzed by tracking the microspheres displacement within the sample. Finally, the techniques used to measure the local swelling of the structure will be correlated with an m-file routine that uses Delaunay triangulations to find the distance of the neighboring microspheres.

4.1. Soft Lithography Delimitations and Approaches

The fabrication of SU-8 microstructures (see Figure 4-3) required the overcoming of several challenges that have been mentioned along this thesis. These process obstacles and complications resulted in SU-8 delaminating,

feature alteration, underdevelopment as well as overdevelopment. All of these problems can be associated with the spinning, ramping velocities, exposure time, and development time. As you can see, each part of the process presented a certain degree of challenge. Feature roughness was highly sensitive to variations in exposure uniformity, which arose from SU-8 thickness, non-uniformity as well as non-uniform contact between photo mask and the SU-8 layer. Therefore, special care was taken at the initial of the soft bake period especially for thicknesses higher than 25 µm. In addition, the bead formation during the spinning step was highly characterized in order to minimize the bead removal process which can be pretty invasive to the SU-8. Moreover, the contact between the photo mask and SU-8 was decreased at maximum by upgrading from an initial process which used to use hard contact to a process in which vacuum was used in order to maximize contact and minimize air diffraction.

On the other hand, the total thickness of the SU-8 microstructure was another important variable in exposure uniformity. In addition, optimizing exposure dosage (power and time) also improved the exposure uniformity. Crack-like distortions (wrinkles or cracks) that manifest during the post-exposure bake can result from underexposure of the SU-8. Finally, bake temperatures, developing time, and agitation played a significant role at the time of characterizing the process of fabricating the SU-8 microstructures.

63

4.2. 3D Reconstruction

There were several parameters that had to be considered before acquiring a z-series suitable for 3D reconstruction in order to obtain a stack with minimal distortions.

4.2.1. Fluidic Chamber Considerations

It was necessary to employ the greatest care when preparing a sample for 3-D reconstruction. Improper sample preparation will produce distorted 3-D images. It is important to notice that the further one focuses in the z-axis of the sample, the more prominent loss of contrast and shadowing become so that upper bright planes appear dim, while lower ones are bright. As you can see from Figure 4-4, (A) shows the z-axis of the microspheres closest to the lens; these microspheres appear larger than the ones from a higher z position (B). One could increase the illumination intensity to overcome some of the problem, yet photobleaching may become severe.

4.3. Image Registration

Another requirement for the effective 3-D reconstruction is image registration. Each optical section of the z-series must be in register with its

64

neighbors during image acquisition; otherwise distortion is introduced into the 3-D reconstruction. Hence, care must be taken to prevent the specimen from moving during the acquisition of the z-series. Since the heating of the chamber is done by flowing hot air through the sample, the chamber had to be sealed on the top. On the other hand, it was not possible to take measurements on the confocal microscopy when the microstructures where fabricated without the TPM binder since there was not a relative structure where to focus the microscope at.

4.4.   Pixel Resolution

A third important consideration before obtaining a z-series is the pixel resolution for the conditions used (objective, magnification, etc) so that the proportional dimensions of the specimen are maintained during the 3D reconstruction. For example, in Figure 4-5 (A), too few sections were taken resulting in a squashed, three-dimensional reconstruction (also, refer to Figure 4-6 which shows an actual example from our data). In (B) the pixel resolution in the xy plane was used to generate the correct distance to obtain optical sections in the z axis. As expected, a near-perfect sphere is expected. (C) Shows that in this example too many optical section were taken, and the sphere appears stretched after three-dimensional reconstruction.

65

4.5. Image Processing of the Stacks

In order to obtain a 3D reconstruction of the microstructure there are some steps that should be considered if one is working with ImageJ. First, the stack should be downloaded as an image sequence. Then, a minimum and a maximum threshold should be applied in order to reduce background noise. In the data shown in this thesis a 15% threshold is set relative to the maximum in each image. After the background noise has been clear out with the threshold tool on ImageJ, we can proceed to find the x, y, and z positions of the microspheres. This was done by choosing a region of interest (ROI) through out the stack (the ROI will be a single trench) (see Figure 4-7). Once the ROI is selected one can proceed to crop this region, so only the microspheres inside the trench will be accounted in the calculations. This will reduce the amount of time ImageJ takes to calculate the coordinates. Finally, using the ImageJ algorithm called "3D Object Counter" the volume, the surface area, the intensity and the coordinates of the spheres is calculated.

4.6. Delaunay Triangulations Results

As mentioned in the previous chapter, a Delaunay triangulation algorithm obtained from Matlab was used to calculate the mean distribution of the microspheres in the network. Figure 4-8 (A) and (B) shows the Matlab output from the Delaunay triangulation algorithm of a poly(NIPAAm) trench that has 15

www.manaraa.com

µm gap between trenches and 10 µm width. (C) and (D) shows the histogram of the distances between the microspheres. The calculated mean distance for (A) was 4.97 µm and 2.85 µm for (B); this is a significant 57% difference between the swollen and collapse state.

Figure 4-11, and Figure 4-12 show the mean distance of microspheres in different trenches widths (for additional information please refer to Figure 4-9 and Figure 4-10). Also, the gaps between the trenches are changed in order to characterize the closing and opening of these trenches.

4.7.   Measuring Local Swelling

Another useful application of the method presented here entails the calculation of the local swelling of the microstructure by sectioning along the z-axis (refer to Figure 4-13). By dividing the z-axis into several sections one can calculate the mean distance of the microspheres in those sections. This method is especially useful in trying to understand how different patterns of surface-attached microstructures of poly(NIPAAm) swelled and collapse along their z-axis. Figure 4-14 shows the Matlab plots of a 52 µm microstructure below the LCST that was divided into four sections. The mean distance of the microspheres and the standard error of the mean were calculated in order to understand the swelling behavior of the trench in each section. The trench in this example came from a PDMS mold with a gap distance of 15 µm, a width of 10 µm, and a

67

thickness of 25 μm. The mean distance of the microspheres in the four sections indicates that the trench reaches a maximum swelling approximately three fourths of its thickness. This behavior resembles a mushroom like shape like the ones reported by Castellanos (2007).

4.8.   Conclusions

The successful attachment of surface-attached poly(NIPAAm) networks to the glass surface was illustrated with spinning-disk confocal microscopy images. In addition, the Delaunay triangulation algorithm obtained from Matlab was proven to successfully calculate the mean distribution of the microspheres in the network. Mean distance of microspheres in different trenches widths and thicknesses was calculated in order to understand the trenches separation influence in the swelling of the patterned hydrogels. These measurements create, for the first time, swelling maps of the structures based on relative movements of fluorescent microspheres. This information will ultimately aid in understanding how swollen macroscopic structures are related to gradients in localized swelling

Furthermore, the quantitative data from this technique may be used to verify the validity of existing hydrogel expansion and contraction models or lead to development of refined theories regarding hydrogel response.

68

Finally, although this set of techniques has been demonstrated for a thermo-responsive hydrogel, its application is not limited only to this class of materials. It can also be applied to hydrogels engineered to respond to other external stimuli, such as ph, light, etc. In addition, this technique could possibly be used on other translucent materials utilized in the construction of more intelligent device designs.
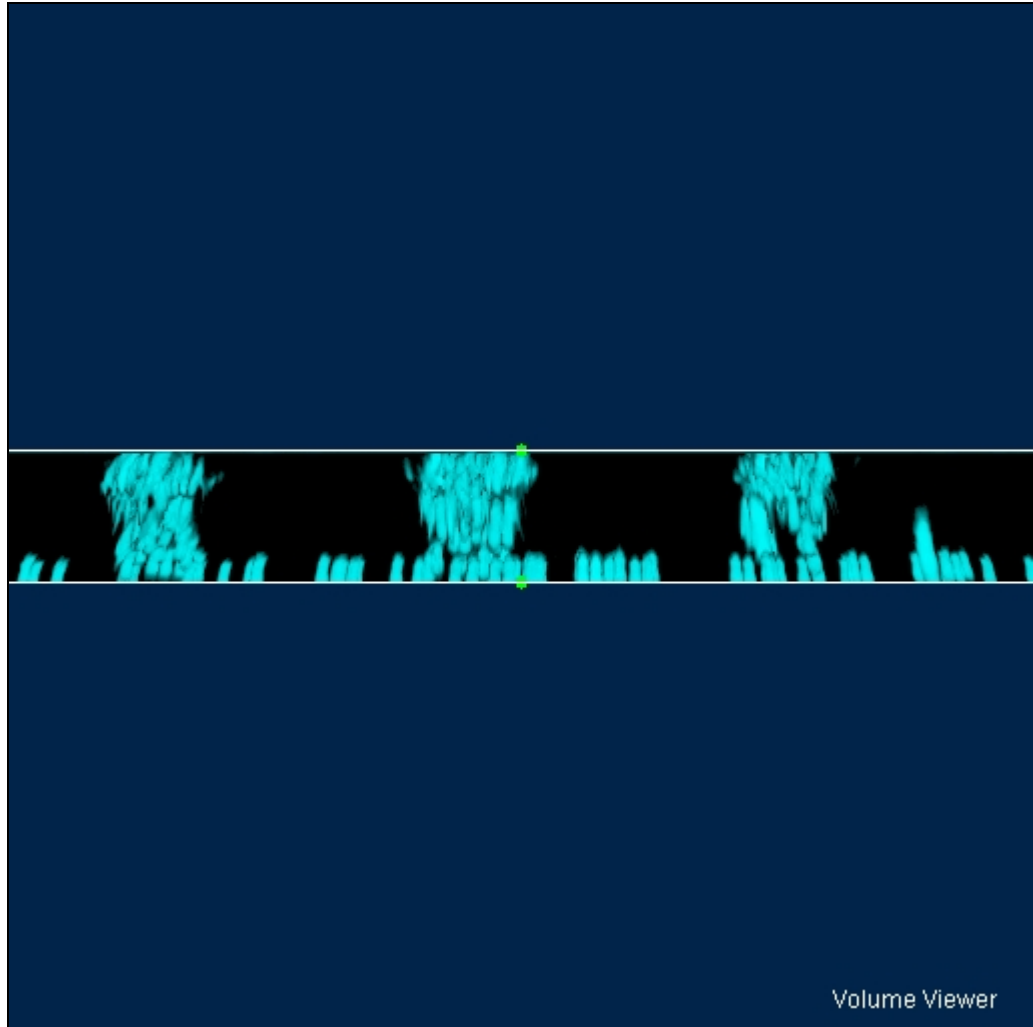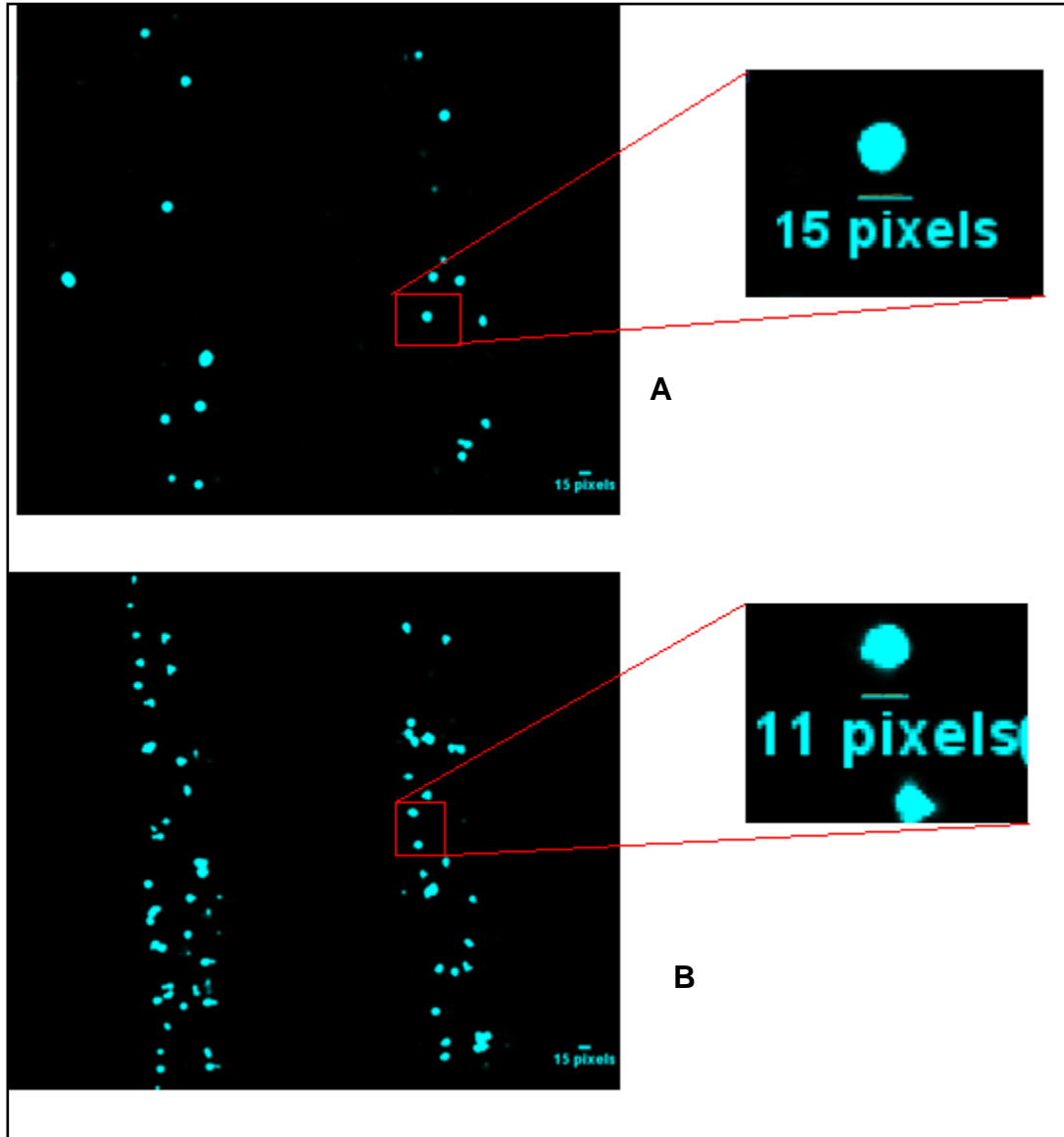
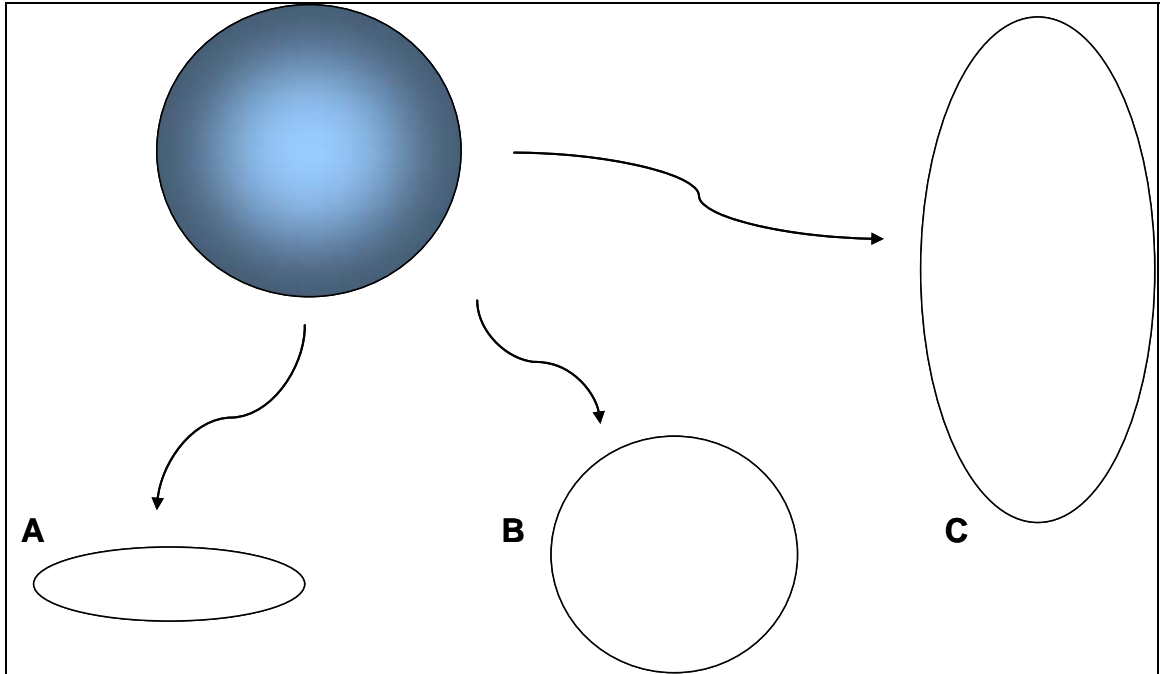**Figure 4-1.** Cross-sectional area of trenches

70
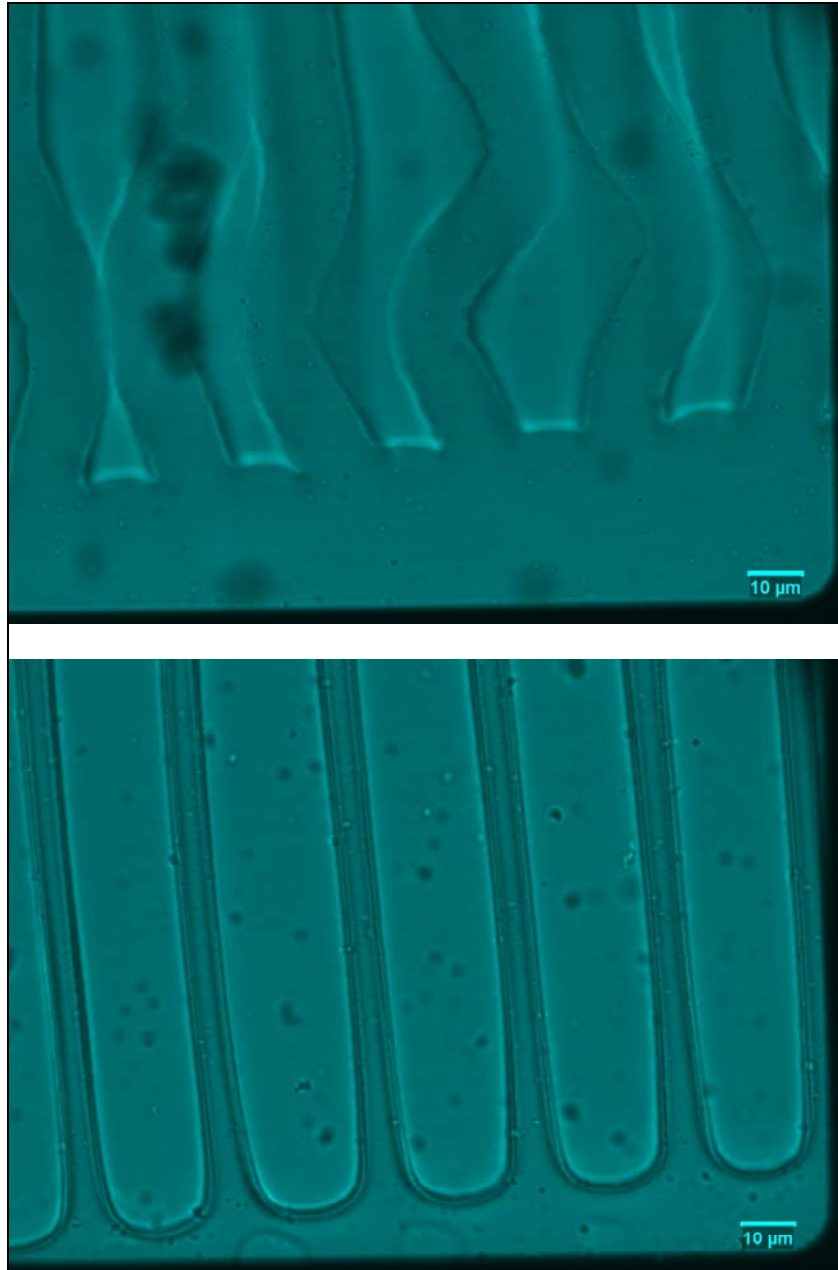
Figure 4-2. Un-buckling of trenches below and above the LCST
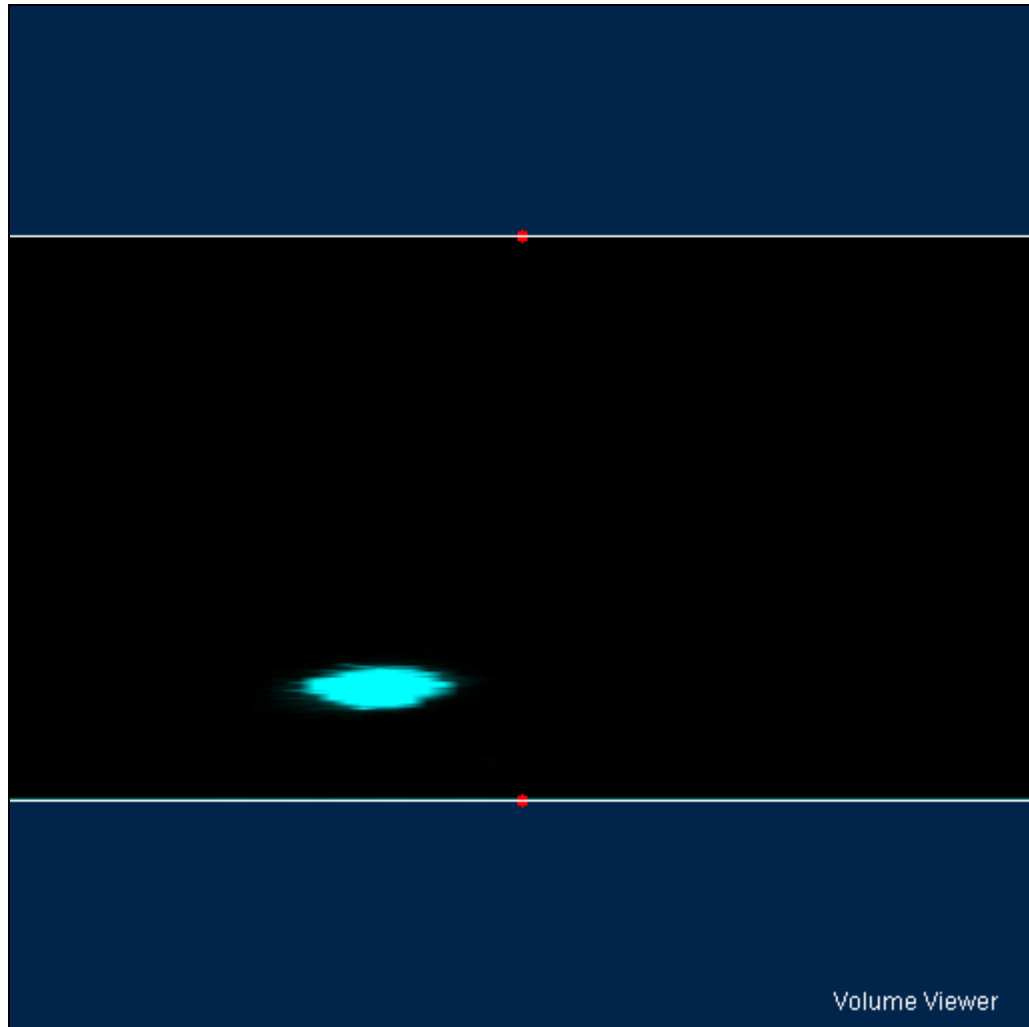
71

Figure 4-3. SU-8 patterned silicon wafer

Figure 4-4. Loss of contrast between lower and upper focal planes

Figure 4-5. Three-dimensional reconstruction of a spherical fluorescent microsphere

Figure 4-6. Cross-sectional view of microspheres where too few optical sections were taken resulting in a squashed, three-dimensional reconstruction

75

A.

B.

C.
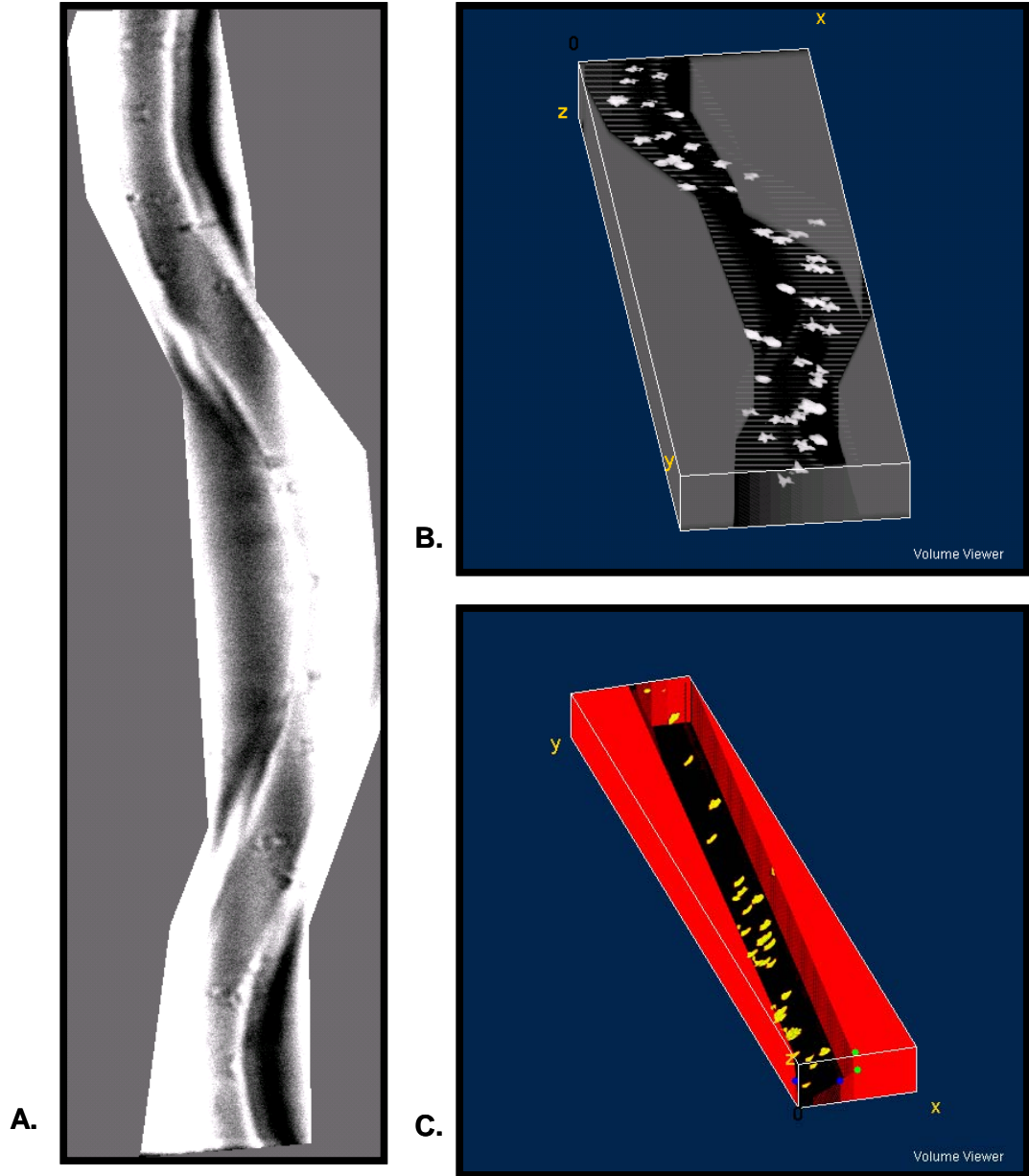
Figure 4-7. Bright field and 3D images of isolated trench below and above the LCST. Cropped trench from a bright field image (A). 3D image from below (B) and above (C) the LCST
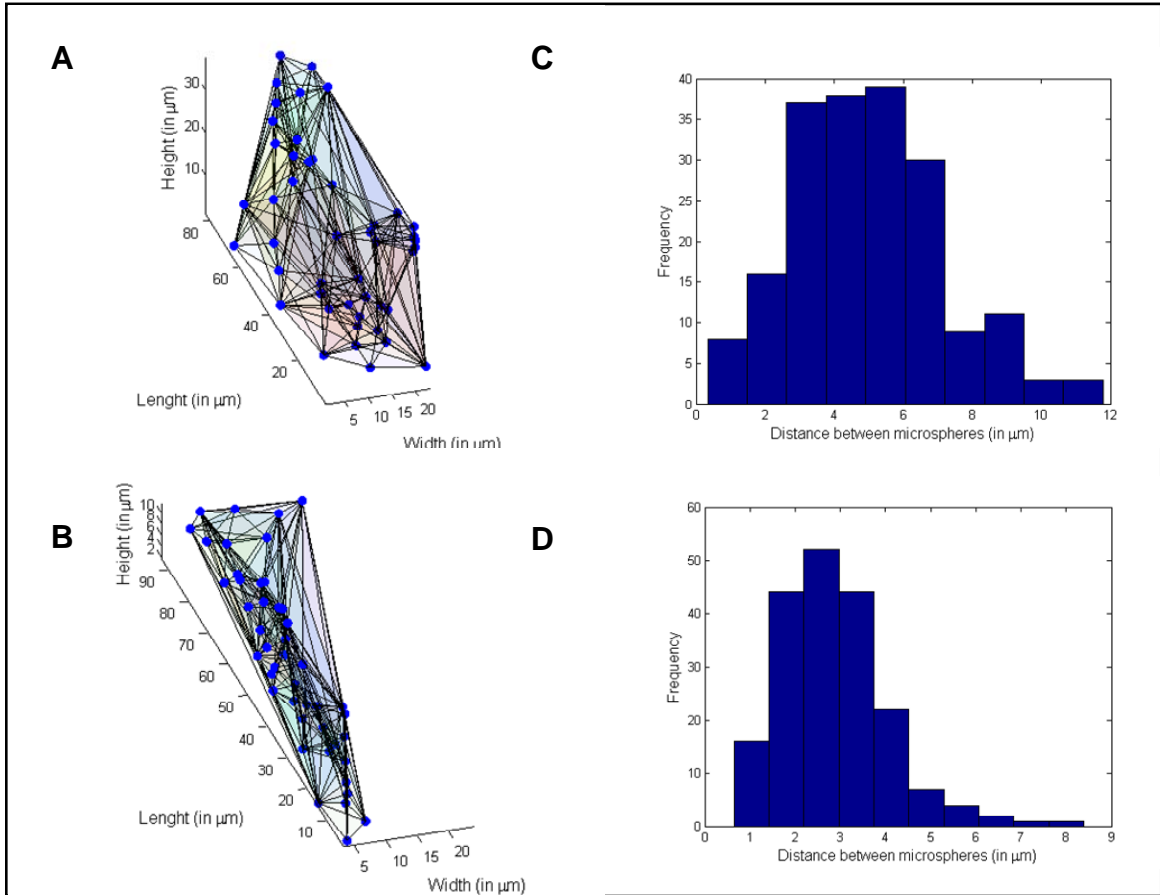
Figure 4-8. Delaunay triangulation of a poly(NIPAAm) trench (A) below (B) above the LCST
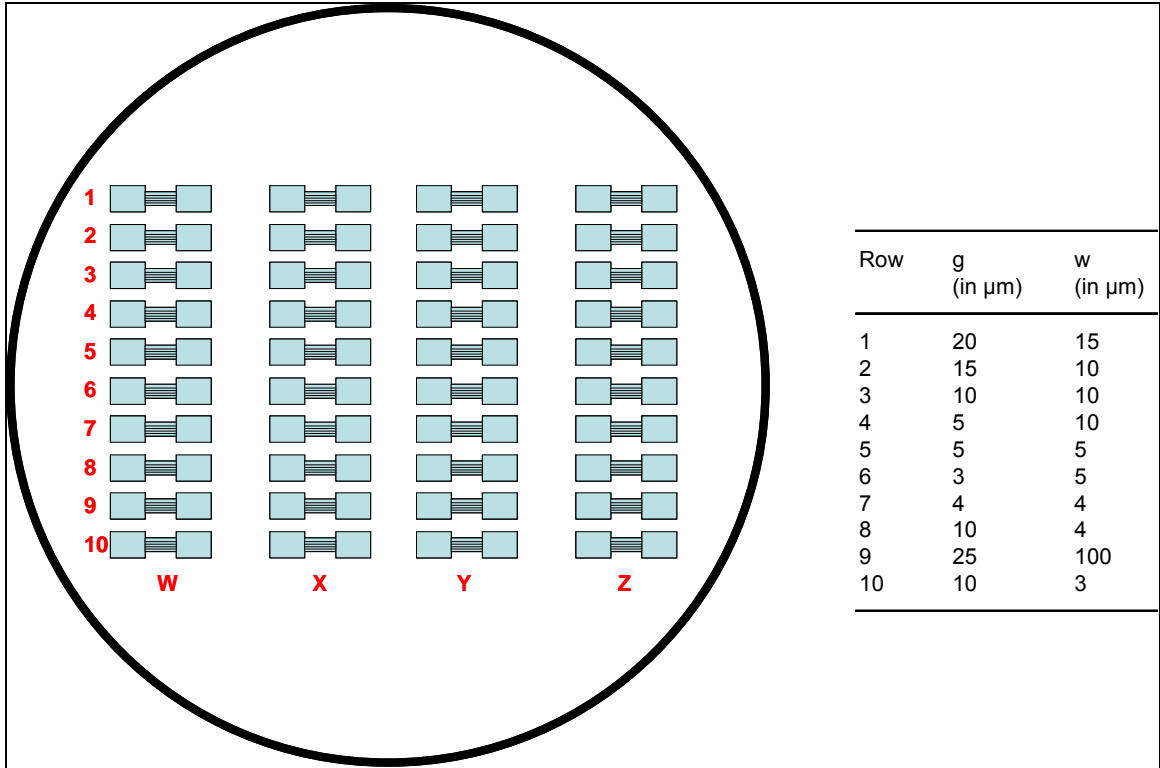
Figure 4-9. Mask with different trenches widths and gaps
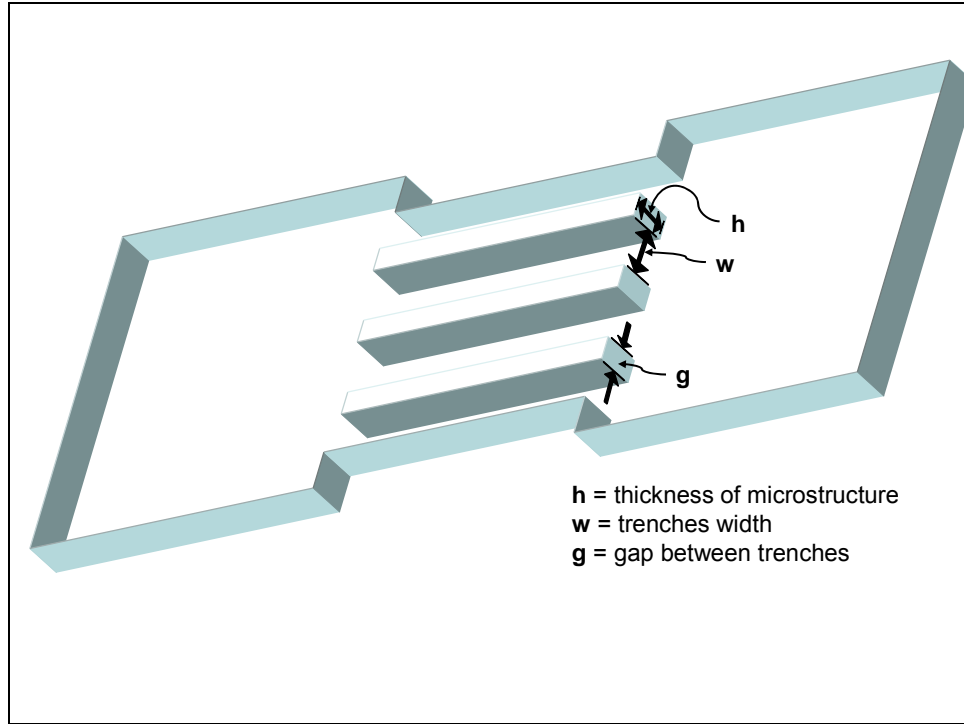
Figure 4-10. 3D of microstructure patterns

In the figure:

h = thickness of microstructure
w = trenches width
g = gap between trenches
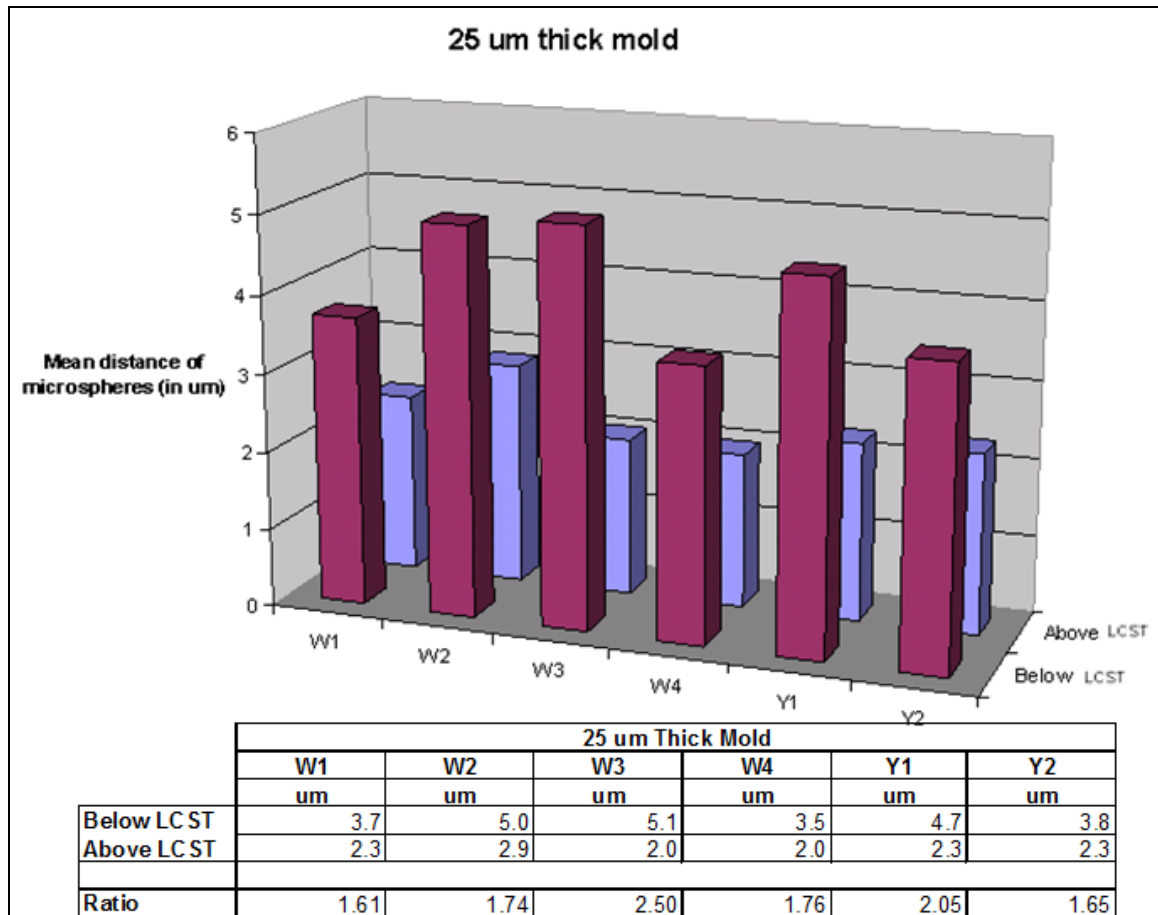
Figure 4-11. Mean distance of microspheres vs. different size trenches widths and gaps (25 um thick mold)

5 um Thick Mold				
	Y1	**Y2**	**Y4**	**Y5**
	um	um	um	um
Below LCST	3.4	3.2	2.3	2.5
Above LCST	2.5	2.3	1.9	2.4
Ratio	1.37	1.37	1.22	1.03
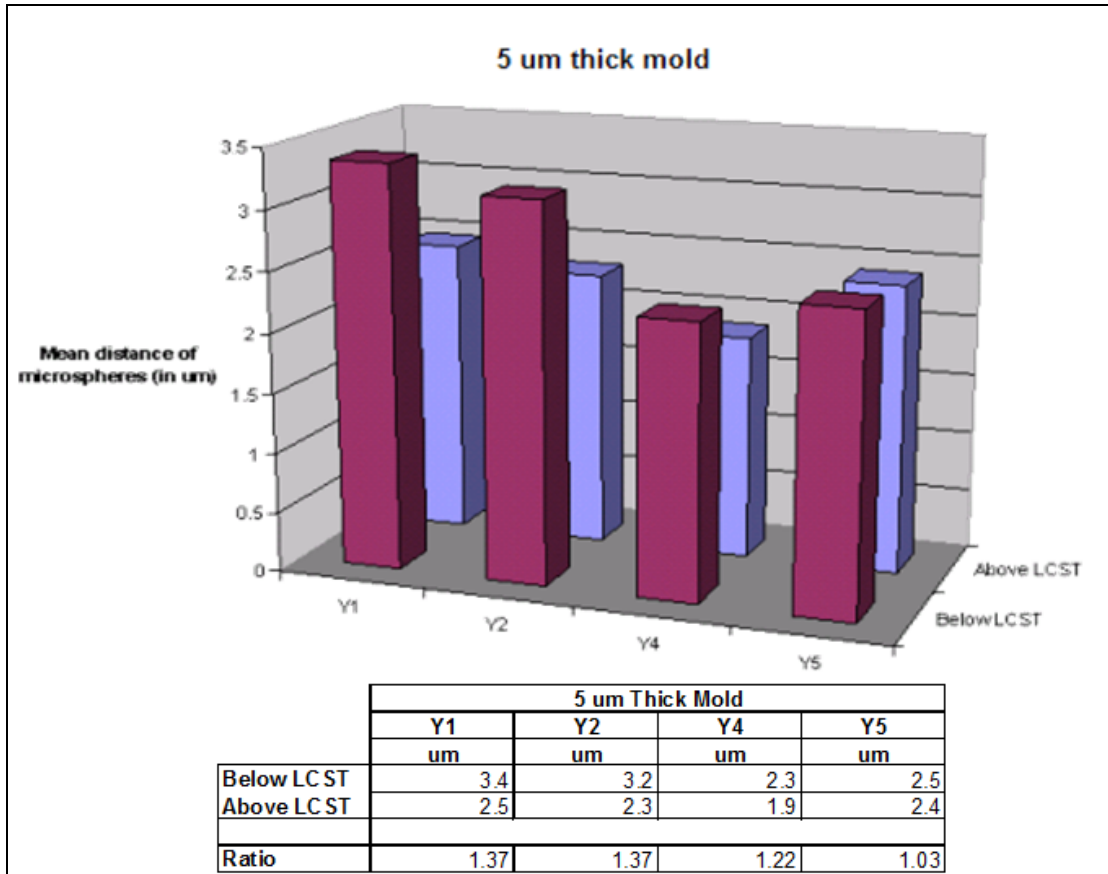
Figure 4-12. Mean distance of microspheres vs. different size trenches widths and gaps (5 um thick mold)

81
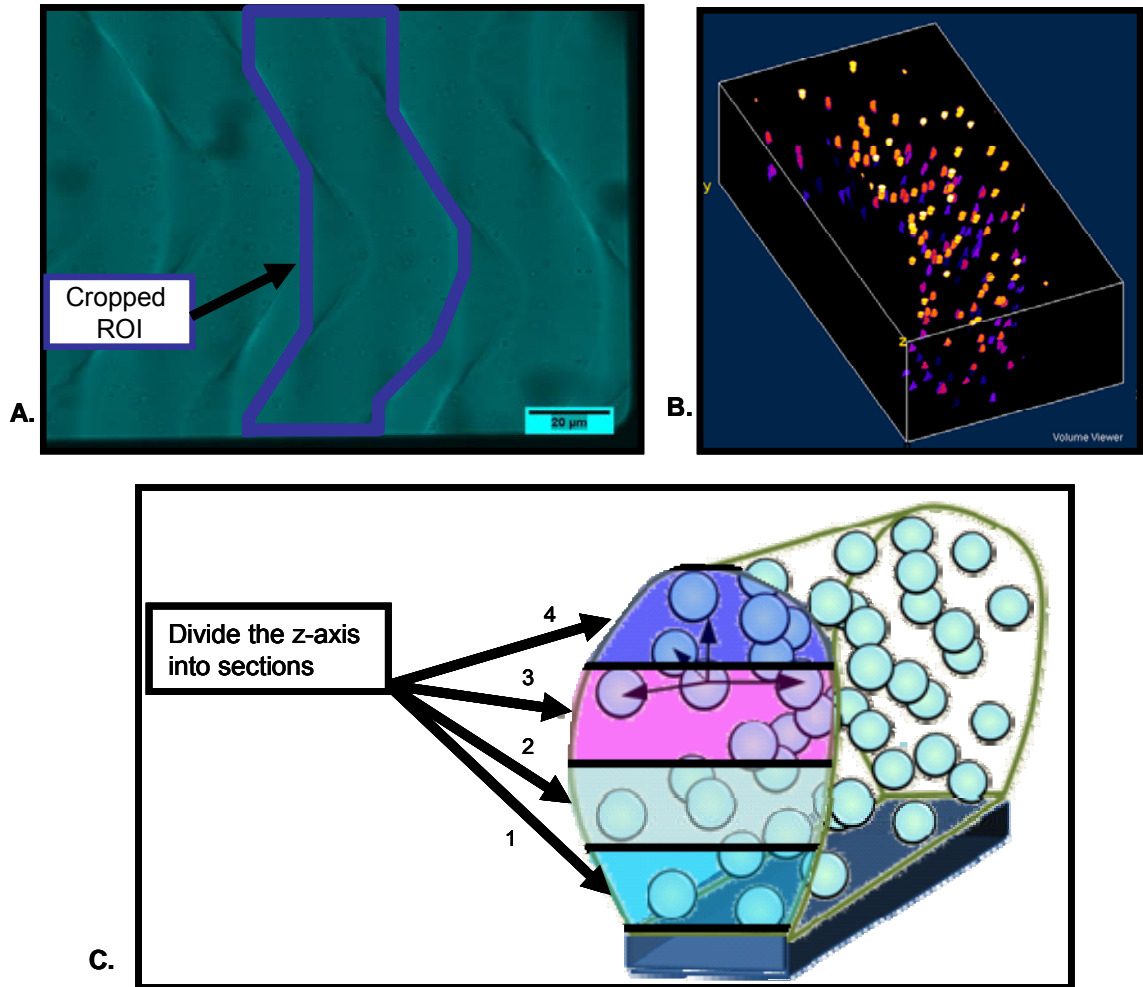
Figure 4-13. Steps to measure the local swelling in different sections of the microstructure. Crop ROI (**A**). Arrange stack in 3D (**B**). Divide z-axis into sections and calculate microsphere distances in these sections (**C**)

82
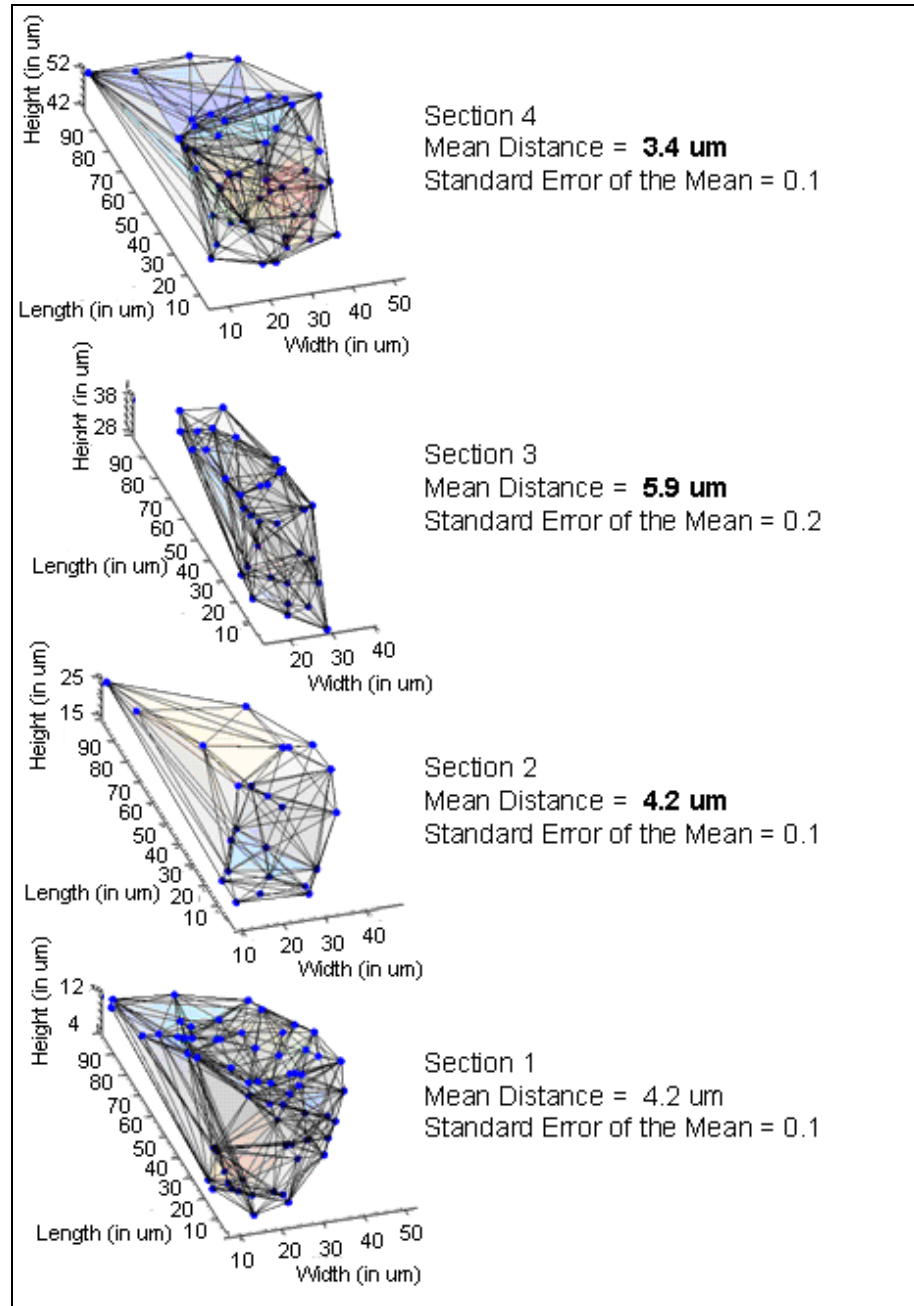
Figure 4-14. Calculating mean distance of microspheres in different z-sections

REFERENCES

1.   J. Hoffmann, M. Plotner, D. Kuckling and W. J. Fischer, Photopatterning of thermally sensitive hydrogels useful for microactuators. *Sens. Actuator A-Phys.*, 1999, 77, (2), 139-144.

2.   H. Tanaka, H. Tomita, A. Takasu, T. Hayashi and T. Nishi, Morphological And Kinetic Evolution Of Surface Patterns In Gels During The Swelling Process - Evidence Of Dynamic Pattern Ordering. *Phys. Rev. Lett.*, 1992, 68, (18), 2794-2797.

3.   A. Suzuki, M. Yamazaki and Y. Kobiki, Direct observation of polymer gel surfaces by atomic force microscopy. *Journal of Chemical Physics*, 1996, 104, (4), 1751-1757.

4.   A. Suzuki, S. Yoshikawa and G. Bai, Shrinking pattern and phase transition velocity of poly(N-isopropylacrylamide) gel. *Journal of Chemical Physics*, 1999, 111, (1), 360-367.

5.   B. H. Jo, L. M. Van Lerberghe, K. M. Motsegood and D. J. Beebe, Three-dimensional micro-channel fabrication in polydimethylsiloxane (PDMS) elastomer. *Journal of Microelectromechanical Systems*, 2000, 9, (1), 76-81.

6.   A. Castellanos, S. J. DuPont, A. J. Heim, G. Matthews, P. G. Stroot, W. Moreno and R. G. Toomey, Size-exclusion "capture and release" separations using surface-patterned poly(N-isopropylacrylamide) hydrogels. *Langmuir*, 2007, 23, (11), 6391-6395.

7.   A. Bertsch, S. Jiguet and P. Renaud, Microfabrication of ceramic components by microstereolithography. *Journal of Micromechanics and Microengineering*, 2004, 14, (2), 197-203.

84

8. P. A. Clerc, L. Dellmann, F. Gretillat, M. A. Gretillat, P. F. Indermuhle, S. Jeanneret, P. Luginbuhl, C. Marxer, T. L. Pfeffer, G. A. Racine, S. Roth, U. Staufer, C. Stebler, P. Thiebaud and N. F. de Rooij, Advanced deep reactive ion etching: a versatile tool for microelectromechanical systems. *J. Micromech. Microeng.*, 1998, 8, (4), 272-278.

9. Y. Hanein, C. G. J. Schabmueller, G. Holman, P. Lucke, D. D. Denton and K. F. Bohringer, High-aspect ratio submicrometer needles for intracellular applications. *J. Micromech. Microeng.*, 2003, 13, (4), S91-S95.

10. J. L. Wilbur, R. J. Jackman, G. M. Whitesides, E. L. Cheung, L. K. Lee and M. G. Prentiss, Elastomeric optics. *Chem. Mat.*, 1996, 8, (7), 1380-1385.

11. J. A. Rogers, R. J. Jackman, O. J. A. Schueller and G. M. Whitesides, Elastomeric diffraction gratings as photothermal detectors. *Appl. Optics*, 1996, 35, (34), 6641-6647.

12. Y. N. Xia and G. M. Whitesides, Soft lithography. *Annual Review of Materials Science*, 1998, 28, 153-184.

13. A. Mata, A. J. Fleischman and S. Roy, Fabrication of multi-layer SU-8 microstructures. *J. Micromech. Microeng.*, 2006, 16, (2), 276-284.

14. R. S. Kane, S. Takayama, E. Ostuni, D. E. Ingber and G. M. Whitesides, Patterning proteins and cells using soft lithography. *Biomaterials*, 1999, 20, (23-24), 2363-2376.

15. K. L. Chavez and D. W. Hess, Removal of resist materials using acetic acid. *Journal of the Electrochemical Society*, 2003, 150, (4), G284-G291.

16. A. Revzin, R. J. Russell, V. K. Yadavalli, W. G. Koh, C. Deister, D. D. Hile, M. B. Mellott and M. V. Pishko, Fabrication of poly(ethylene glycol) hydrogel microstructures using photolithography. *Langmuir*, 2001, 17, (18), 5440-5447.

17. W. G. Koh, A. Revzin, A. Simonian, T. Reeves and M. Pishko, Control of mammalian cell and bacteria adhesion on substrates micropatterned with poly(ethylene glycol) hydrogels. *Biomedical Microdevices*, 2003, 5, (1), 11-19.

18. H. Lorenz, M. Despont, N. Fahrni, J. Brugger, P. Vettiger and P. Renaud, High-aspect-ratio, ultrathick, negative-tone near-UV photoresist and its applications for MEMS. *Sens. Actuator A-Phys.*, 1998, 64, (1), 33-39.

19. K. D. Vora, B. Y. Shew, E. C. Harvey, J. P. Hayes and A. G. Peele, Specification of mechanical support structures to prevent SU-8 stiction in high aspect ratio structures. *J. Micromech. Microeng.*, 2005, 15, (5), 978-983.

20. J. Zhang, M. B. Chan-Park and S. R. Conner, Effect of exposure dose on the replication fidelity and profile of very high aspect ratio microchannels in SU-8. *Lab on a Chip*, 2004, 4, (6), 646-653.

21. C. H. Lin, G. B. Lee, B. W. Chang and G. L. Chang, A new fabrication process for ultra-thick microfluidic microstructures utilizing SU-8 photoresist. *Journal of Micromechanics and Microengineering*, 2002, 12, (5), 590-597.

22. E. H. Conradie and D. F. Moore, SU-8 thick photoresist processing as a functional material for MEMS applications. *J. Micromech. Microeng.*, 2002, 12, (4), 368-374.

23. C. L. Cromer, T. B. Lucatorto, T. R. Obrian and M. Walhout, Improved dose metrology in optical lithography. *Solid State Technology*, 1996, 39, (4), 75-78.

24. J. Tien, C. M. Nelson and C. S. Chen, Fabrication of aligned microstructures with a single elastomeric stamp. *Proc. Natl. Acad. Sci. U. S. A.*, 2002, 99, (4), 1758-1762.

25. K. Kim, D. S. Park, H. M. Lu, W. Che, J. B. Lee and C. H. Ahn, A tapered hollow metallic microneedle array using backside exposure of SU-8. *J. Micromech. Microeng.*, 2004, 14, (4), 597-603.

26.   J. Carlier, S. Arscott, V. Thomy, J. C. Fourrier, F. Caron, J. C. Camart, C. Druon and P. Tabourier, Integrated microfluidics based on multi-layered SU-8 for mass spectrometry analysis. *J. Micromech. Microeng.*, 2004, 14, (4), 619-624.

27.   M. B. Chan-Park, J. Zhang, Y. H. Yan and C. Y. Yue, Fabrication of large SU-8 mold with high aspect ratio microchannels by UV exposure dose reduction. *Sensors and Actuators B-Chemical*, 2004, 101, (1-2), 175-182.

28.   Y. J. Chuang, F. G. Tseng and W. K. Lin, Reduction of diffraction effect of UV exposure on SU-8 negative thick photoresist by air gap elimination. *Microsystem Technologies*, 2002, 8, (4-5), 308-313.

29.   M. C. Peterman, P. Huie, D. M. Bloom and H. A. Fishman, Building thick photoresist structures from the bottom up. *J. Micromech. Microeng.*, 2003, 13, (3), 380-382.

30.   X.-Z. Zhang, G.-M. Sun and C. C. Chu, Temperature sensitive dendrite-shaped PNIPAAm/Dex-Al hybrid hydrogel particles: formulation and properties. *European Polymer Journal*, 2004, 40, (9), 2251-2257.

31.   B. Bohl, R. Steger, R. Zengerle and P. Koltay, Multi-layer SU-8 lift-off technology for microfluidic devices. *J. Micromech. Microeng.*, 2005, 15, (6), 1125-1130.

32.   H. K. Chang and Y. K. Kim, UV-LIGA process for high aspect ratio structure using stress barrier and C-shaped etch hole. *Sens. Actuator A-Phys.*, 2000, 84, (3), 342-350.

33.   J. D. Williams and W. Wang, Microfabrication of an electromagnetic power relay using SU-8 based UV-LIGA technology. *Microsyst. Technol.*, 2004, 10, (10), 699-705.

34.   J. Wang and Z. Chen, Self-Actuated, Thermo-Responsive Hydrogel Valves for Lab on a Chip. *Biomedical Microdevices*, 2005, 7, (4), 313-322.

87

35. J. M. K. Ng, I. Gitlin, A. D. Stroock and G. M. Whitesides, Components for integrated poly(dimethylsiloxane) microfluidic systems. *Electrophoresis*, 2002, 23, (20), 3461-3473.

36. A. D. Stroock, S. K. W. Dertinger, A. Ajdari, I. Mezic, H. A. Stone and G. M. Whitesides, Chaotic mixer for microchannels. *Science*, 2002, 295, (5555), 647-651.

37. W. H. Grover, A. M. Skelley, C. N. Liu, E. T. Lagally and R. A. Mathies, Monolithic membrane valves and diaphragm pumps for practical large-scale integration into glass microfluidic devices. *Sens. Actuator B-Chem.*, 2003, 89, (3), 315-323.

38. H. Takao, K. Miyamura, H. Ebi, M. Ashiki, K. Sawada and M. Ishida, A MEMS microvalve with PDMS diaphragm and two-chamber configuration of thermo-pneumatic actuator for integrated blood test system on silicon. *Sens. Actuator A-Phys.*, 2005, 119, (2), 468-475.

39. E. Delamarche, H. Schmid, B. Michel and H. Biebuyck, Stability of molded polydimethylsiloxane microstructures. *Adv. Mater.*, 1997, 9, (9), 741-746.

40. P. Silberzan, L. Leger, D. Ausserre and J. J. Benattar, SILANATION OF SILICA SURFACES - A NEW METHOD OF CONSTRUCTING PURE OR MIXED MONOLAYERS. *Langmuir*, 1991, 7, (8), 1647-1651.

41. R. Banga, J. Yarwood, A. M. Morgan, B. Evans and J. Kells, FTIR AND AFM STUDIES OF THE KINETICS AND SELF-ASSEMBLY OF ALKYLTRICHLOROSILANES AND (PERFLUOROALKYL)TRICHLOROSILANES ONTO GLASS AND SILICON. *Langmuir*, 1995, 11, (11), 4393-4399.

42. J. B. Brzoska, I. Benazouz and F. Rondelez, Silanization of Solid Substrates - a Step toward Reproducibility. *Langmuir*, 1994, 10, (11), 4367-4373.

43. D. Kim and D. J. Beebe, Hydrogel-based reconfigurable components for microfluidic devices. *Lab Chip*, 2007, 7, (2), 193-198.

44. M. J. Park, W. M. Choi and O. O. Park, Patterning polymer light-emitting diodes by micromolding in capillary. *Current Applied Physics*, 2006, 6, (4), 627-631.

45. N. F. Sheppard, M. J. Lesho and P. McNally, MICROFABRICATED CONDUCTIMETRIC PH SENSOR. *Sens. Actuator B-Chem.*, 1995, 28, (2), 95-102.

46. L. E. Helseth and T. M. Fischer, Fundamental limits of optical microrheology. *Journal of Colloid and Interface Science*, 2004, 275, (1), 322-327.

47. T. Tanaami, S. Otsuki, N. Tomosada, Y. Kosugi, M. Shimizu and H. Ishida, High-speed 1-frame/ms scanning confocal microscope with a microlens and Nipkow disks. *Appl. Optics*, 2002, 41, (22), 4704-4708.

48. M. C. Adams, W. C. Salmon, S. L. Gupton, C. S. Cohan, T. Wittmann, N. Prigozhina and C. M. Waterman-Storer, A high-speed multispectral spinning-disk confocal microscope system for fluorescent speckle microscopy of living cells. *Methods*, 2003, 29, (1), 29-41.